

ESTABLISHING THE DLR-F25 AS A RESEARCH BASELINE AIRCRAFT FOR THE SHORT-MEDIUM RANGE MARKET IN 2035

Sebastian Wöhler¹, Jannik Häßy² & Vivian Kriewall³

¹German Aerospace Center (DLR), Institute of System Architectures in Aeronautics, Hamburg, 21129, Germany
 ²German Aerospace Center (DLR), Institute of Propulsion Technology, Cologne, 51147, Germany
 ³Hamburg University of Technology, Institute of Aircraft Systems Engineering, Hamburg, 21129, Germany

Abstract

Investigating the impact of disruptive aircraft technologies and liquid hydrogen along with the associated propulsion and system architectures for the next generation of aircraft leads to the need to compare and benchmark innovative aircraft concepts with a meaningful conventional aircraft configuration. In order to establish such a configuration with a corresponding technology scenario in 2035 for research programs such as the German Luftfahrtforschungsprogramm (LuFo), the Clean Aviation Program and Horizon Europe, the LuFo project VirEnfREI is developing a research baseline configuration for the short-to-medium range segment.

Keywords: Overall Aircraft Design, Research Baseline, Short-Medium Range

1. Motivation

In the context of the European Green Deal and the objective of achieving climate neutrality by 2050 [1], a major research challenge in aviation is the investigation of the impact of liquid hydrogen as energy source and the associated propulsion and system architectures as well as other disruptive aircraft technologies to further increase aircraft efficiency, as depicted in Figure 1. As the short-medium range segment is the largest contributor to CO2 emissions in aviation, accounting for more than 50 % [2], a single-aisle aircraft was selected for detailed investigation.

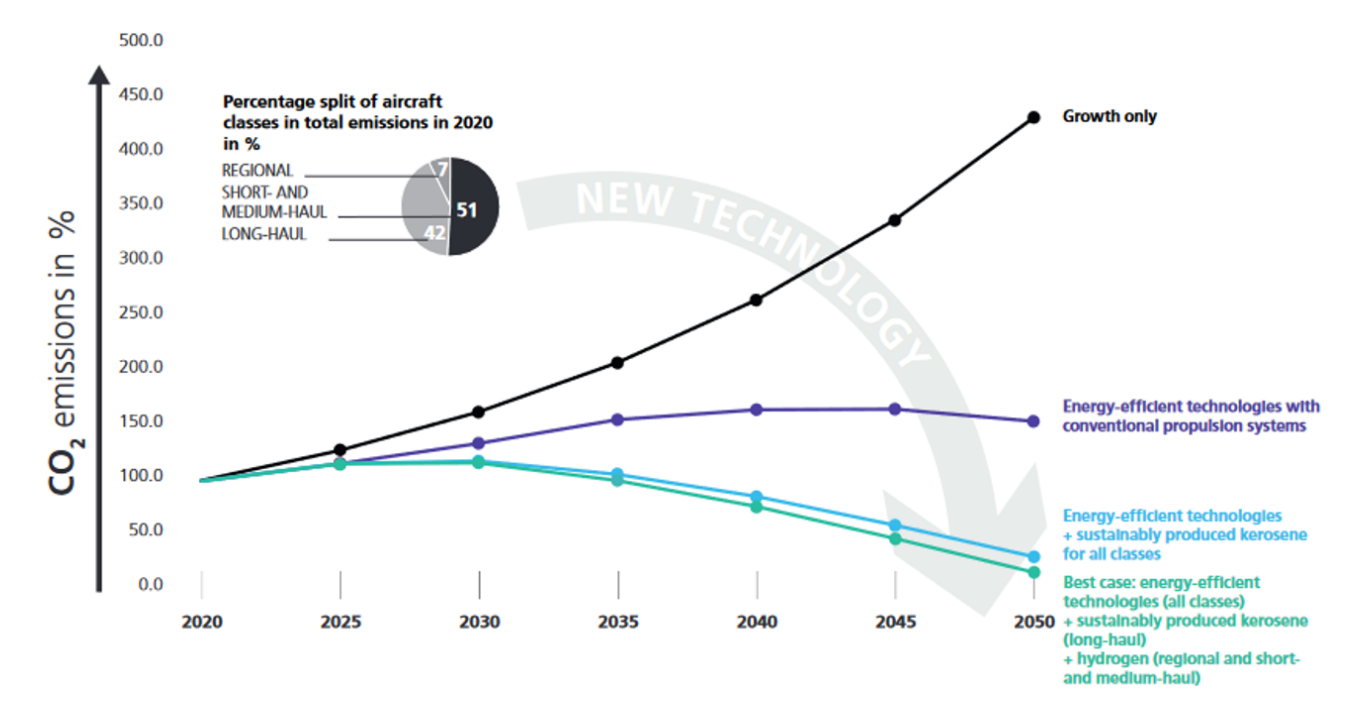


Figure 1 – Technology potential for curbing carbon dioxide emissions retrieved from [2]

For the application of these technologies in the next generation of aircraft, these activities lead to the need to compare and benchmark corresponding aircraft concepts with a meaningful conventional aircraft configuration in order to identify the advantages and disadvantages of each technology or aircraft concept. To establish such a configuration with a corresponding technology scenario, which is expected to be available in 2035 for a kerosene research baseline configuration, the DLR-F25 for the short-medium range (SMR) market segment is being developed within the German funded Luftfahrtforschungsprogramm (LuFo) project VirEnfREI. The goal of the VirEnfREI project is to apply the Cybermatrix approach [3] developed at DLR for multidisciplinary design optimization under industrial specifications and boundary conditions and to demonstrate the associated benefits. Therefore, an initial starting point and use case for the planned activities was needed to demonstrate the optimization process. As not only the VirEnfREI project requires a meaningful point of reference for benchmarking and investigation of the design process and technology application, the DLR-F25 configuration is also used as a starting point for research activities in numerous Clean Aviation, LuFo, Horizon Europe and DLR internal research projects. The various projects investigate different research topics of the configuration such as aerodynamic and structural wing design, high lift design, on-board system design, engine design and integration, as well as advanced load alleviation and active flutter suppression concepts on a very high aspect ratio wing on a common aircraft definition as complementary work. Therefore, the design process and rationale behind the DLR-F25 aircraft design is described in detail to establish the DLR-F25 as a research baseline aircraft to be widely applied to reduce the initial effort for each individual research project to design a conventional evolutionary aircraft concept as point of comparison.

2. Methodology

The aircraft design process is carried out in several iterations in line with the various projects involved. Since the engine and on-board systems design are not directly integrated into the overall aircraft design process, several design loops were performed and the results of the individual design processes described hereafter were integrated for each aircraft design iteration.

2.1 Aircraft Design Environment

The applied aircraft design and sizing process is based on the established multifidelity and multidisciplinary aircraft design environment developed at DLR [4] and applied in various aircraft design projects. It is built around the DLR's conceptual aircraft design tool openAD [4] and utilizes the RCE framework [5] to execute the aircraft design workflow between the different DLR institutes and disciplines involved. For the data exchange between the different heterogeneous tools and scripts hosted on the individual institute's servers, the CPACS data format [6] is used for a continuous and consistent exchange of aircraft data and requirements.

To execute the aircraft design workflow, top-level aircraft requirements (TLARs) and aircraft design parameters are required to define the aircraft configuration. As this study focuses on a conventional approach, the design space for this study is limited to a tube and low wing aircraft configuration with wing mounted engines. In addition to the aircraft design parameters, TLARs and on-board systems definition, engine performance characterisation, geometry and mass definition is required, and is derived separately from the detailed engine design process to be integrated into the aircraft design loop.

2.2 Engine Design Process

The detailed conceptual engine design is carried out using the virtual propulsion framework GTlab [7, 8, 9]. The DLR performance program (DLRp2) is used for thermodynamic cycle analysis. The multidisciplinary workflow for engine sizing is shown in figure 2 and implements a multi-point design approach. Thrust requirements as well as power and bleed off-takes are prescribed for take-off, end of field, second segment, top of climb and cruise conditions. Thermodynamic cycle parameters are estimated to provide the requested thrust and off-takes at all defined operating conditions and without exceeding technological limits. Based on the resulting thermodynamic engine data, a knowledge-based procedure is applied for flow path sizing and engine mass is estimated by means of part-based semi-empirical correlations as described in [10] and applied in [11]. A simple aerodynamic

analysis is conducted based on geometrical flow path parameters and thermodynamic cycle data to estimate velocity triangles and averaged flow and loading coefficients for each turbo component. A correlation approach is used to predict the polytropic component efficiencies accounting for entry into service, operational conditions, component loading and size as presented in [12]. Spool speeds are determined by maximum limiters for turbine disk load and circumferential speeds at the inlet of compressors and the outlet of the low-pressure turbine. Spool speeds and predicted efficiencies are fed back into all disciplinary models and a fixed point iteration is used to find a convergent solution. An emission model is applied to estimate engine emissions similar to [11, 13]. A more detailed overview of engine model assumptions and design constraints is presented in [11].

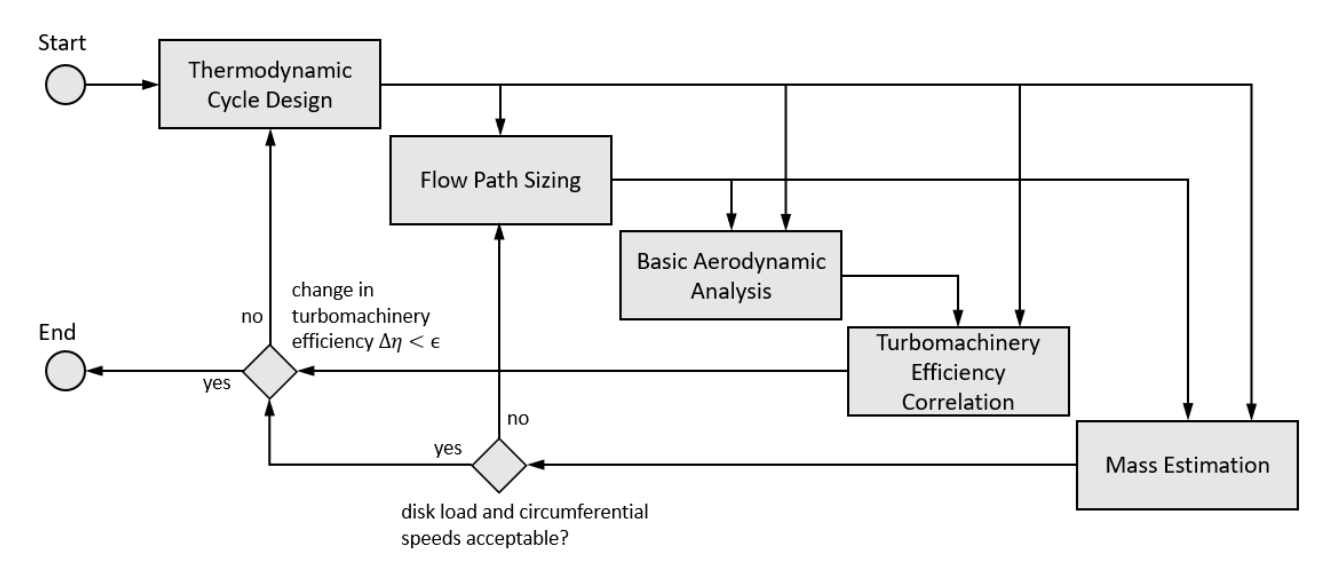


Figure 2 – Workflow for multidisciplinary conceptual engine design

For the selected engine design, engine ratings are defined and performance maps that contain the operational regime between minimum and maximum rated thrust in dependence on Mach number and altitude are calculated. These engine performance maps as well as engine dimensions and mass are provided to the aircraft design process. The engine sizing is repeated manually until the thrust requirements from overall aircraft design are converged.

2.3 On-Board Systems Design Process

As a fundamental aspect of the overall aircraft design (OAD) process, the aircraft on-board systems (OBS) architecture is initially defined, with the selection of appropriate system technologies. Subsequently, the individual systems as part of the overall systems architecture are conceptually sized. In order to achieve this objective, the Overall Systems Design (OSD) framework developed by the Institute of Aircraft Systems Engineering at Hamburg University of Technology (TUHH) is employed. As illustrated in Figure 3, the OSD framework is integrated into the OAD process and detailed systems design (DSD) methods, such as further transient system analysis. The OSD framework comprises two methods:

- 1. Systems Architecture Assistant (SArA) for OBS architecture definition [14, 15, 16, 17]
- 2. GeneSys for preliminary systems sizing and simulation [18, 19, 20, 21]

The input for the OSD framework is comprised of the TLARs and the parametric description of the aircraft geometry as part of the aircraft CPACS file. Subsequently, *SArA* is employed to create a functional-logical representation of the aircraft's overall systems architecture through the application of model-based systems engineering (MBSE) approaches. Here, the *Matlab System Composer* is utilized [22]. Consequently, the *SArA* model encompasses the relevant system components and functional-logical connections between them. In fact, the employment of *SArA* results in the generation of a pool of systems architecture variants comprising different technologies. Alternatively,

known architecture variants can be retrieved from a connected database. A reduction in the number of functional-logical architecture variants to one or two promising candidates for further analysis and conceptual design within GeneSys is conducted. This is achieved by employing criteria such as safety, complexity, and risk [16]. Thus, no physics-based sizing is conducted at this stage. The selected *SArA* architectural model is saved in an XML-based file, which is subsequently transferred to *GeneSys* for the actual preliminary sizing procedure of the OBS.

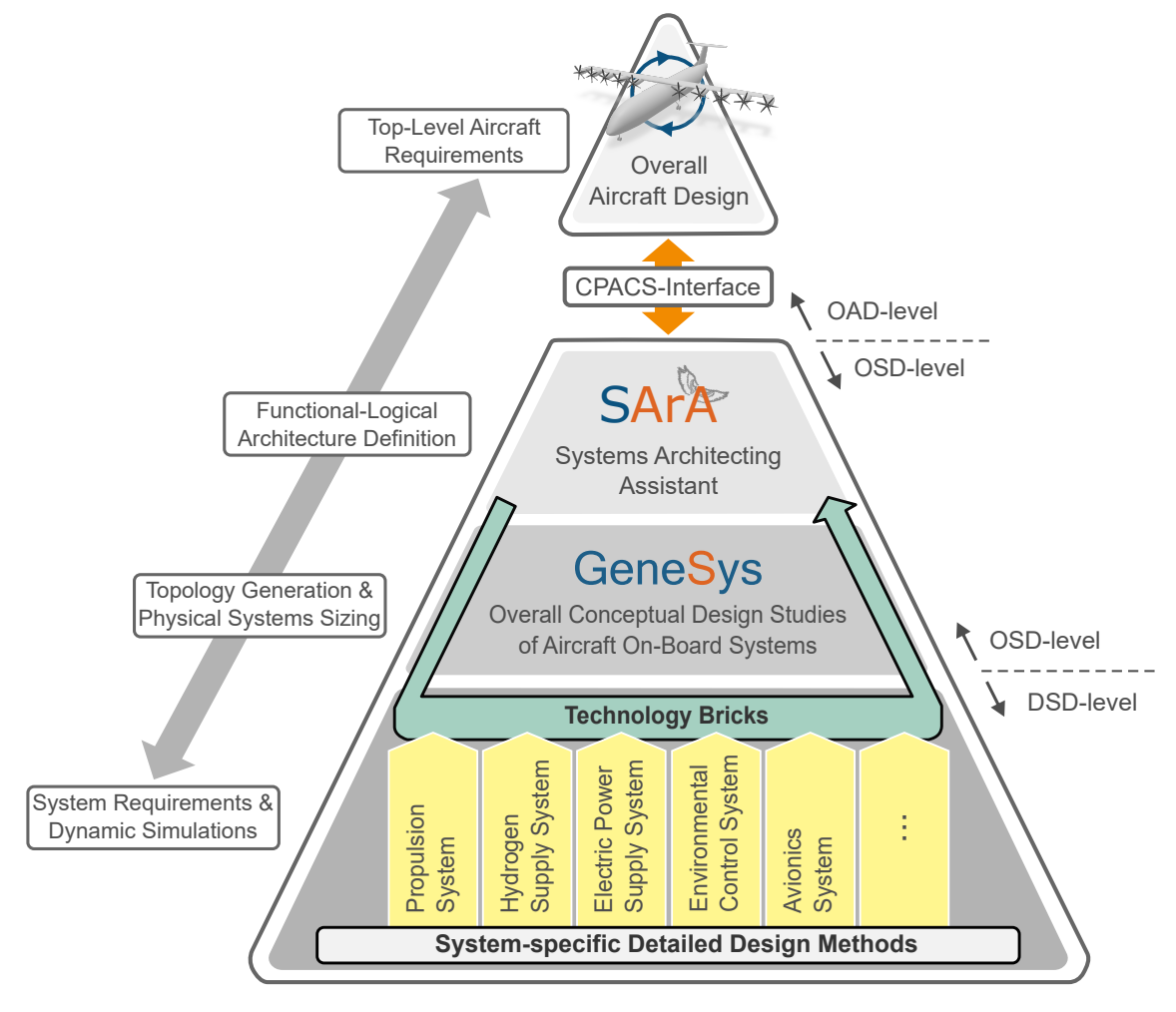


Figure 3 – Embedded overall systems design (OSD) framework in the overall aircraft design (OAD) and the detailed systems design (DSD)

The GeneSys method begins with the generation of the topology of the systems architecture. In this initial step, the system components are positioned within the given aircraft geometry. Furthermore, as defined in the SArA model, physical connections, such as ducts, pipes, and electric cables, are routed between the components. For the positioning of components and connections, a knowledge-based approach is employed. However, for the routing of the electric power supply system, an auto-routing algorithm is used [19]. As part of the subsequent parametric physics-based sizing procedure, the consumer systems, such as hydraulic actuators, air conditioning packs, and electric consumers, are initially sized based on the typical load cases that are applicable to the considered aircraft or the power requirements specified by OAD. Subsequently, the masses of the systems' components are estimated using component-specific mass scaling laws, which are based on the design power of the component. Secondly, the power supply systems, which conventionally are pneumatic, hydraulic, or electric, are sized using a graph-based approach. The design power values of the consumer components or systems are aggregated at junctions and propagated through the power supply system network to the sources. This allows the source components, such as the hydraulic pump or electric generator, to be sized. Finally, based on the known design parameters of the system components, an off-design quasi-static, forward-directed mission simulation is performed using a reference mission

profile as part of the aircraft CPACS file. Defined mission parameters, such as flight altitude, Mach number, flight phase, and flight control surface and gear control parameters, are employed to estimate the power consumption of the on-board systems, that is, the bleed air and shaft power off-takes at the engines, throughout the mission profile. The system topology and sizing results, including masses, center of gravity, power demands, and lengths of connections are stored as part of an XML-based ontology file. This enables the exchange of data with OAD and DSD disciplines.

2.4 Top-Level Aircraft Requirements

The TLARs are the key constraints for the development of the next generation of aircraft. During the aircraft design, the TLARs are identified, documented and continuously tracked to ensure that the required performance is achieved. In the conceptual design phase, the TLARs constrain the design space and define performance targets. Reference for the VirEnfREI project is the Airbus A321neo as of 2020 technology status as the representative aircraft for today's short-medium range market segment. For the next generation of aircraft, key technologies and aircraft configurations will be identified to support the introduction of a new product by 2035. As the VirEnfREI project does not carry out specific market research to identify specific requirements for a potential market scenario in 2035, the TLARs are therefore derived from the reference aircraft to ensure consistency and appropriate comparison and are summarised in the Table 1.

Table 1 – TLARs for the 2035 short-medium range aircraft based on the Airbus A321neo [23]

Parameter	Unit	Value
Design Range	[nm]	2500
Design PAX (single class)	[-]	239
Mass per PAX	[kg]	95
Design Payload	[kg]	25000
Max. Payload	[kg]	25000
Cruise Mach number	[-]	0.78
Max. operating Mach number	[-]	0.82
Design dive speed	[kts]	380
Maximum operating speed	[kts]	350
Max. operating altitude	[ft]	40000
TOFL (ISA +0K SL)	[m]	2200
Rate of Climb @ TOC	[ft/min]	>300
Approach Speed (CAS)	[kt]	136
Wing span gate limit	[m]	<36
Alternate Distance	[nm]	200
Holding Time	[min]	30
Contingency	[-]	3%

The design PAX number is taken from the reference aircraft based on a high-density layout as depicted in Figure 4 retrieved from [24]. For comparison, the cabin layout with its comfort standard and the resulting outer geometry of the fuselage cockpit and constant section is kept fixed for this study. The design range of the aircraft to be achieved with the design payload is defined by 2500nm. This range is subject to marketing studies and future market forecasts and is taken from the reference [23]. As the market forecast is not investigated in the VirEnfREI project, it is assumed that the market requirements will remain the same as for the A321neo. Thus, the next generation of aircraft in the short medium range market studied in the scope the VirEnfREI project is designed as a direct replacement. Increased ranges can be achieved by reducing the design payload up to the ferry range of an aircraft. The design payload of 25000kg is the maximum payload and includes a mass of 95kg per PAX and an additional margin for growth, cargo and future developments.

The cruise Mach number of 0.78 is typical for short medium range operations and the maximum operating Mach number is defined by cruise Mach number + 0.04. The Mach number can be part of

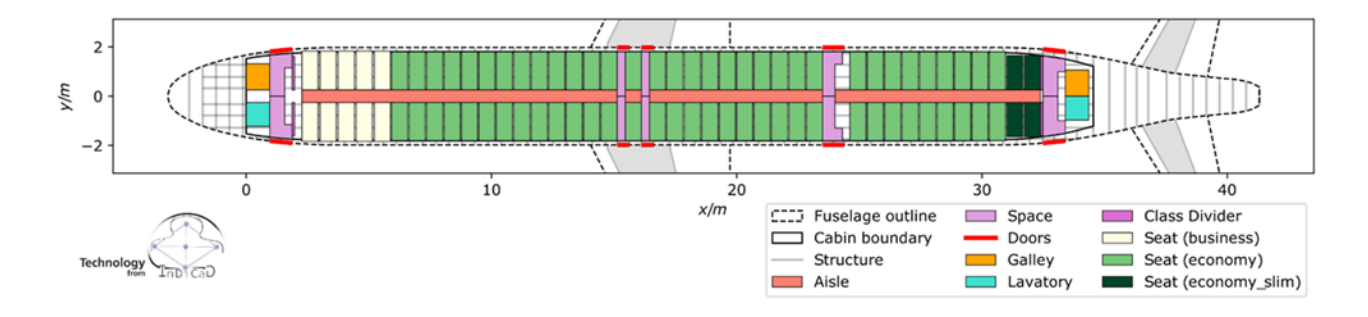


Figure 4 – 239-seat layout of an Airbus A321neo similar aircraft based on a sketch by Airbus as found in [23] and retrieved from [24]

design trade studies to optimize the aircraft design with respect to different propulsion architectures, such as the open rotor concept. Design speed and maximum operating speed are defined as the design criteria up to which the aircraft must withstand structural loads and were chosen based on the reference aircraft. The maximum operating altitude is also initially taken from the reference as well, but may be adjusted if the design and performance benefits justify it. The maximum operating altitude determines the engine design requirements, as well as the aerodynamic performance and the cabin differential pressure, and thus the structural design, with countervailing effects on the overall block energy efficiency of the airframe. The rate of climb at top of climb (TOC) ensures sufficient performance reserves to respond to air traffic restrictions and collision avoidance maneuvers. The approach speed of 136kts is initially taken from the reference in order to maintain the same approach speed category as the reference aircraft [23, 25]. In consideration of future growth potential, the maximum approach speed within the category of 141kts has not been selected, but may be subject to future adjustments [26].

Airport compatibility requires a gate limit of less than 36m. This can be achieved by a variable wing geometry such as by folding wing tips, novel approaches to park the aircraft within the airport gate box or other technical measures to reduce the overall wing span at the gate.

For the reserve mission, a distance of 200nm to an alternate airport in the SMR segment is defined in accordance with the CS-25, as well as the requirement to ensure 30 minutes holding time for emergency procedures. The contingency to be considered in the design corresponds to 3% of the trip fuel due to, among other factors, worse than expected engine performance or unfavorable weather conditions.

2.5 Technology Assumptions

The aircraft component technology factors and rationales are summarized in Table 2 and are applied during the conceptual design phase of the DLR-F25 configuration and represent a conventional evolutionary design approach for a low wing aircraft configuration with wing mounted engines. They are derived from various research projects and are aligned with the IATA "Aircraft Technology Roadmap to 2050" [27]. The indicated mass technology factors are not mass saving factors over the D239 component masses, the DLR design of a 239 seat (see Figure 4) aircraft similar to the Airbus A321neo, but rather a technology calibration factor for a similar component in shape and size.

The engine performance improvement is based on the detailed studies presented in Chapter 3. For the initial design of the aircraft, a calibration factor was applied to the reference engine to derive the initial thrust requirements for the detailed engine design. For the final sizing of the DLR-F25, the specific engine performance characterisation for the entire flight envelope was applied.

For the fuselage, the application of advanced aluminium alloys and advances in manufacturing and assembly methods are considered within the -5% technology factor. The use of CFRP is not considered for the single-aisle architecture due to the relatively larger cut-outs compared to the widebody application and the resulting inferior mass saving potential at higher manufacturing costs. The same reasoning applies to the empennage, with a lower technology factor, as the horizontal and vertical tailplanes are already made of CFRP [23].

Table 2 – Technology assumptions applied during conceptual aircraft design phase

Component	Technology Factor	Rationale
Engine Performance	+4%	Compared to a 2015 state-of-the-art geared turbo fan, Bypass-ratio: 15 and improved thermal efficiency
Fuselage Mass	-5%	Compared to D239 Advanced Al-alloys, manufacturing and assembly methods,
Empennage Mass	-3%	but also revised production and certification requirements Compared to D239 Advanced manufacturing and assembly methods
Wing Mass	-30%	Compared to D239 Application of CFRP, advanced load alleviation, active flutter suppression, adaptive dropped hinge flaps and foldable wing tips
System Mass	-5%	On-board system architecture based on design by TUHH
Furnishing Mass Operator Items Mass	ISO ISO	Potential mass reductions are mitigated by new requirements and certification rules as well as additional modularity, manufacturability and increased complexity

The key technology, in addition to the ultra high bypass ratio (UHBR) engine, is the high aspect ratio wing design with a span of 45m to study the design and impact of advanced load alleviation, low speed roll control, active flutter suppression and the integration of high lift devices on a very slender wing, also to be tested as a scaled prototype in the wind tunnel as part of the VirEnfREI Project. The stated technology factor takes into account the aforementioned technologies at component level as an initial estimate in the overall aircraft design, which will need to be verified within the framework of the research projects.

The 5% technology factor of the system mass is derived from the detailed on-board system design carried out by the TUHH and described in detail in Chapter 4.

The mass of furniture and operator items is kept constant as the cabin layout is not modified and no significant change in overall mass is expected as described in Table 2.

3. Engine Design

Two different generic engine models are considered in this publication assuming an unmixed geared turbofan architecture for both of them (see figure 5). In order to ensure consistency and comparability between the engine models, the same set of methods and internal calibration factors is applied. Both engines are calculated assuming the fuel Jet-A1 with a lower fuel heating value of 43.25 MJ/kg.

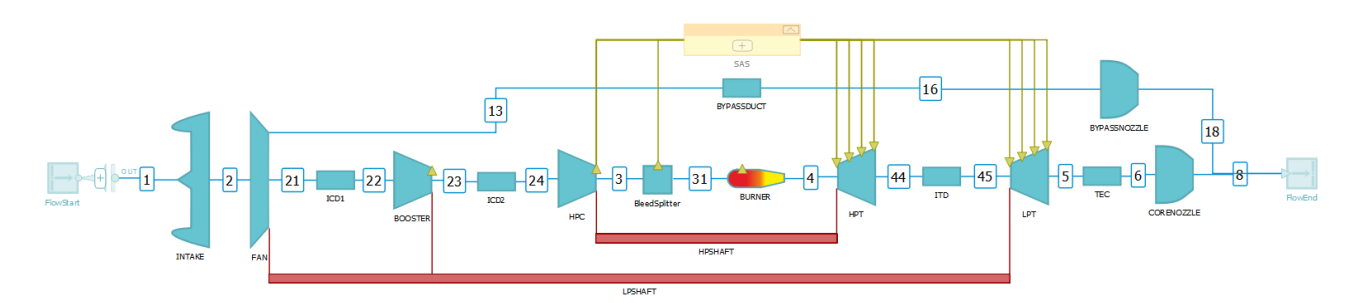


Figure 5 – Schematic for the unmixed geared turbofan architecture

The first engine that is referred to as reference engine powers the D239 aircraft and represents a new production engine of average manufacturing quality with entry into service in 2015. The thermodynamic cycle parameters are selected in order to match data from the ICAO data bank at sea level static conditions. An overview of characteristic engine parameters is provided in table 3 for sizing oprating conditions. At the typical mid cruise point, the D239 engine is operated at a bypass ratio (BPR) of 12.4, an overall pressure ratio (OPR) of 37.6 and has a TSFC of 14.86 g/kN/s.

Table 3 – Overview of engine parameters for the D239 engine

Parameter	Unit	Cruise	TOC	MTO-0	MTO-15	EOF	2ndSeg
Thrust	[N]	21874	28825	147280	147280	116100	105440
Thrust	[lbf]	4917	6480	33110	33110	26100	23704
Mach number	[-]	0.78	0.76	0	0	0.24	0.237
Altitude	[m]	10668	10363.2	0	0	0	122
Flight Level	[100ft]	350	340	0	0	0	4
Temp. Deviation from ISA	[K]	0	10	0	15	15	15
Power Off-Take	[W]	-60000	-110000	-110000	-110000	-110000	-110000
Customber Bleed	[kg/s]	0.425	0.57	0	0	0	0
TSFC	[g/kNs]	14.86	15.37	6.95	7.19	9.88	9.76
TSFC	[lb/lbf/h]	0.525	0.543	0.245	0.254	0.349	0.345
OPR	[-]	37.6	44.9	38.1	38.1	39.0	36.5
BPR	[-]	12.4	11.2	11.6	11.6	11.8	12.0
Fan Face ax. Mach	[-]	0.622	0.684	0.562	0.562	0.591	0.560
Fan Inlet Mass Flow	[kg/s]	241.5	254.8	595.6	580.5	620.1	591.3
FAR	[-]	0.0259	0.0306	0.0304	0.0322	0.0331	0.0317
T3	[K]	758	838	875	915	931	911
T4	[K]	1633	1835	1860	1944	1980	1927
T41	[K]	1519	1707	1732	1812	1845	1796
NOx Flow	[g/s]	3.74	7.37	30.69	44.0	56.1	41.2

The second engine that aims to represent a next generation engine with entry into service in 2035 is dedicated to power the DLR-F25 configuration and is iteratively designed in close exchange with overall aircraft design. Assumed improvements in engine technology are limited to evolutionary technology maturation. The achievable component efficiencies in 2015 and 2035 are modeled according to [12]. Further improvements can be achieved by the selection of characteristic thermodynamic cycle parameters during the design iteration. For the future engine, the maximum stator outlet temperature is limited for the maximum climb rating to $T_{41} = 1725$ K and for the maximum take-off rating to $T_{41} = 2050$ K. The minimum required blade height at the outlet of the high pressure compressor is set to $T_{3} = 1000$ K.

In order to find the optimal future engine design on overall system level, the bypass ratio, overall pressure ratio and turbine entry temperature of the engine are varied using the described multidisciplinary workflow. By means of local sensitivities that are provided by overall aircraft design for the typical mission, reductions in thrust specific fuel consumption $\Delta TSFC$ are traded against additional engine mass ΔM_{eng} and an increased maximum nacelle radius ΔR_{nac} . With equation 1, the relative change in mission fuel burn ΔFB is calculated comparing different engine designs against a reference design.

$$\Delta FB = \frac{\partial FB}{\partial TSFC} \left(TSFC - TSFC_{ref} \right) + \frac{\partial FB}{\partial M} \left(M_{eng} - M_{eng,ref} \right) + \frac{\partial FB}{\partial R_{nac}} \left(R_{nac} - R_{nac,ref} \right) \tag{1}$$

Figure 6 shows exemplary the variation of the bypass ratio (BPR) at cruise. With increasing BPR, the engine accelerates a larger mass flow to a lower level of jet velocity. This leads to a higher propulsive efficiency and a lower thrust specific fuel consumption. The efficiency improvement is degressive with BPR. The fan diameter and also the engine mass grow with BPR counteracting efficiency improvements with respect to block fuel. Applying the sensitivities, the optimal BPR is found to be BPR = 16. For the engine of the DLR-F25, a slightly lower value of BPR \approx 15 is selected as will be discussed in the following paragraph.

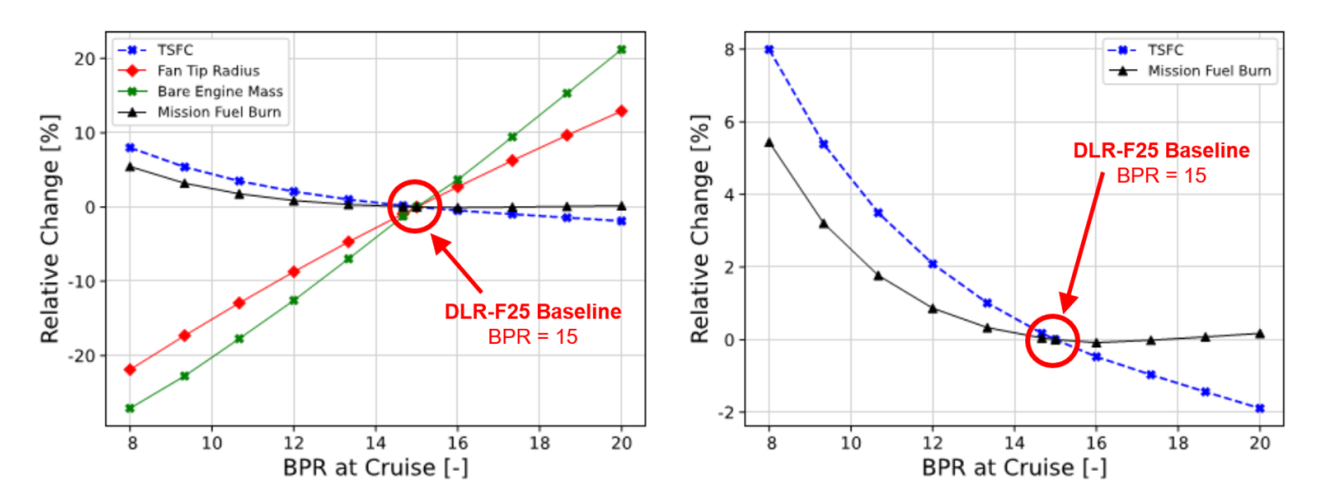


Figure 6 – Variation of the engine bypass ratio at cruise for constant thrust requirements

Since several combinations of bypass ratio, overall pressure ratio and turbine entry temperature lead to a low level of mission fuel burn, the emitted flow of nitrogen oxide emissions (NOx) at cruise conditions is introduced as a second objective. Nitrogen oxide emissions substantially contribute to the climate impact of aviation and should be minimized not only for the landing and take-off (LTO) cycle but also for cruise operation.

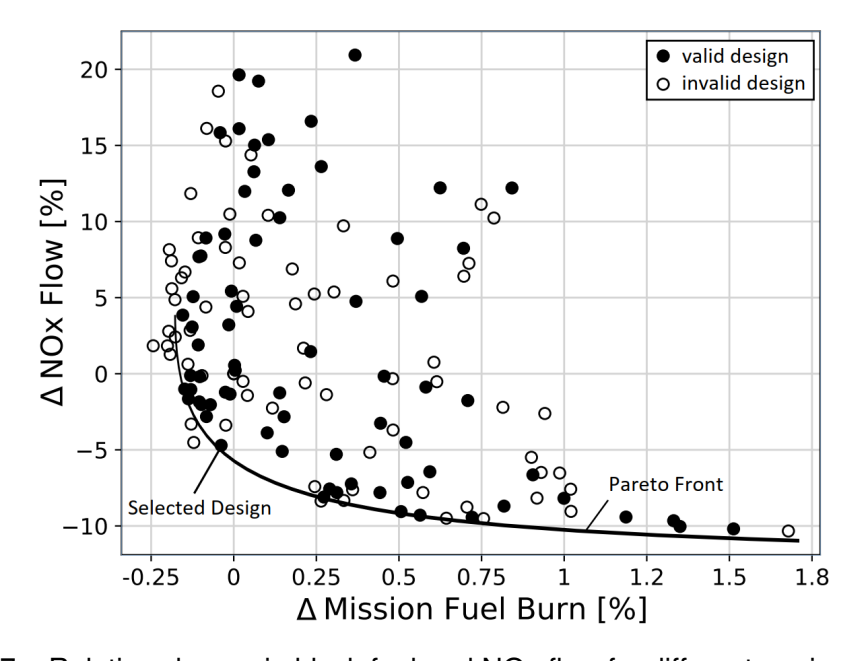


Figure 7 – Relative change in block fuel and NOx flow for different engine designs

Figure 7 shows the relative change of the emitted NOx flow versus the relative change in mission fuel burn for a variation of engine design parameters. The solid samples are feasible engine designs in line with technological limitations. The hollow samples represent invalid engine designs, which exceed the maximum temperature limit at top of climb or have a too small blade height at the outlet of the high pressure compressor. Connecting all valid, dominating designs leads to the Pareto-front in

figure 7. The engine design is selected pareto-optimal allowing fuel burn penalties < 0.25 % in favor of low NOx emissions at cruise operation. With this small penalty, NOx reductions of 5 to 10 % are achievable compared to the design with minimum fuel burn.

Table 4 presents an overview of characteristic engine parameters for the selected engine for the DLR-F25 configuration. At the typical mid cruise point, the DLR-F25 engine is operated at a bypass ratio (BPR) of 15.1, an overall pressure ratio (OPR) of 41.1 and has a TSFC of 14.33 g/kN/s. In order to compare both engines for similar operating conditions, the DLR-F25 engine is evaluated for the cruise conditions (altitude, off-takes) of the D239 maintaining the corrected thrust (FN / T1 * 101325 Pa) of 47.1 kN resulting in a TSFC of 14.34 g/kN/s. Therefore, the thrust specific fuel consumption of the DLR-F25 engine is improved by 3.6 % compared to the reference engine. Please note, the assumed improvements in future engine technology are limited to thermodynamic cycle parameters and evolutionary improvements of component efficiencies. The effect of innovative cycles or revolutionary component technologies is not considered here.

Table 4 – Overview of engine parameters for the DLR-F25 engine

Parameter	Unit	Cruise	TOC	MTO-0	MTO-15	EOF	2ndSeg
Thrust	[N]	17828	23046	124710	124710	86872	76109
Thrust	[lbf]	4008	5181	28036	28036	19530	17110
Mach number	[-]	0.78	0.76	0	0	0.228	0.239
Altitude	[m]	11277.6	11277.6	0	0	11	122
Flight Level	[100ft]	370	370	0	0	0	4
Temp. Deviation from ISA	[K]	0	10	0	15	15	15
Power Off-Take	[W]	-50000	-50000	-95000	-95000	-95000	-95000
Customber Bleed	[kg/s]	0.425	0.425	0	0	0	0
TSFC	[g/kNs]	14.33	14.49	6.25	6.45	8.94	9.05
TSFC	[lb/lbf/h]	0.506	0.511	0.221	0.228	0.316	0.320
OPR	[-]	41.1	49.9	38.0	38.0	35.9	33.0
BPR	[-]	15.1	13.6	14.2	14.2	14.9	15.4
Fan Face ax. Mach	[-]	0.620	0.684	0.503	0.503	0.502	0.476
Fan Inlet Mass Flow	[kg/s]	224.3	227.2	563.2	549.0	564.5	538.6
FAR	[-]	0.0256	0.0298	0.0283	0.0300	0.0295	0.0282
T3	[K]	769	850	872	913	906	885
T4	[K]	1632	1821	1799	1881	1859	1805
T41	[K]	1529	1707	1690	1767	1747	1696
NOx Flow	[g/s]	2.99	5.87	22.95	32.78	29.66	21.30

Figure 8 presents the flow path dimensions and mass for both engines. Even if the DLR-F25 engine has a higher bypass ratio, the fan radius is only 1 cm larger compared to the D239 engine. This is related to the significantly lower thrust requirements of the DLR-F25 aircraft. Due to the higher BPR and less required thrust, the core engine is shorter and lighter in case of the DLR-F25. The bare engine mass is reduced by 9.5 % and the total length of the installed power plant is 5 % shorter even if the DLR-F25 engine has an additional low-pressure turbine stage.

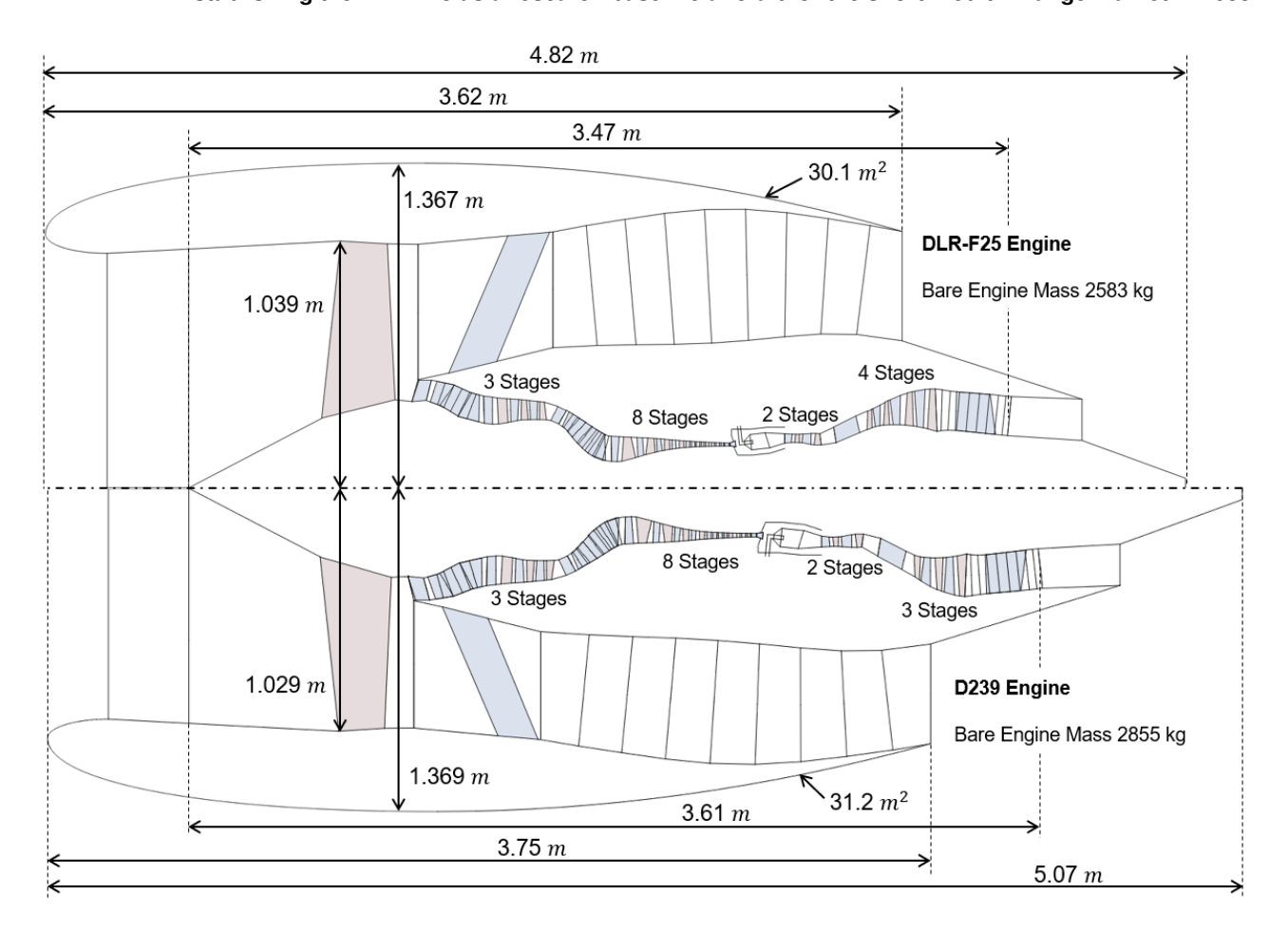


Figure 8 – Flow path model comparison of the D239 and DLR-F25 engine

4. On-Board Systems Design

This section presents the results of the OBS definition and preliminary sizing procedures for the DLR-F25. First, an overview is provided regarding the selected technologies for the individual systems as part of the OBS definition procedure. Second, the sizing results regarding mass and power off-take estimation are outlined.

4.1 Systems Architecture Definition

In order to define the overall system architecture for the DLR-F25, it is necessary to first establish a well-known reference based on an existing state-of-the-art short-medium range aircraft, namely the D239 (cf. Figure 14). Thereby, the OSD tool set is calibrated, which enables the generation of meaningful sizing results for concept aircraft such as the DLR-F25. Subsequently, a contemporary, more-electric systems architecture for the DLR-F25 is developed, incorporating 2035 technology. A notable feature is the more-electric flight control system (FCS) architecture, which incorporates electro-hydrostatic and electro-mechanic actuators. The layout of the FCS for the DLR-F25 is depicted in Figure 9 and is mirrored for the left wing side. Consequently, the hydraulic power supply system comprises two hydraulic circuits (green and yellow) for the DLR-F25, in contrast to the typical number of three hydraulic networks observed in state-of-the-art systems. In addition, the electric power supply system (EPSS) has been modified to align with the latest technological advancements, ensuring its suitability for the FCS electrification. The EPSS features a modern distributed architecture, with a voltage level of 400/230VAC. The characteristics of a distributed EPSS architecture are described by Bielsky et al [18]. The DLR-F25's EPSS comprises two main networks (E1 and E2). Table 5 provides a summary of the selected technologies and components that are applicable to the systems architecture of the DLR-F25.

Table 5 – Selected technologies and composition of the individual on-board systems for the DLR-F25

System	Description
Environmental control system (ECS)	Bleed air-based; single raiser duct architecture; 2 ECS packs including air-cycle machines; 1 cockpit zone; 2 cabin zones (forward and aft)
Flight control system (FCS)	More-electric; see layout in Figure 9)
Ice protection system (IPS)	Bleed air-based wing ice protection system (WIPS) at wing leading edges; electric windshield heaters
Landing gear actuation (LDG)	Hydraulic servo actuators for main and nose LDG legs and doors; hydraulic nose wheel steering; hydraulic brakes (cf. Figure 9)
Lights	Runway turn off, taxiing, take-off, wing illumination, landing, low beacon, up beacon, wing tip strobe, navigation wing, logo, tail strobe, navigation tail, cabin aisle, cabin window
Cabin equipment and furnishings	Luggage bins, linings, ceiling, screen panels, windows, insulation, cockpit door, floor, life jackets, curtains, emergency equipment, cabin and flight crew seats, galleys (oven, coffee machine, storage bins), trolleys, tablets, crew and crew luggage
Auxiliary power unit (APU)	SAF-powered gas turbine
Cargo doors actuation	Hydraulic servo actuators at forward and aft right cargo doors each; supplied by yellow hydraulic circuit (cf. Figure 9)
Fuel system	Pressure-based refuel system; 1 center tank; 1 wing tank left; 1 wing tank right; 2 jet pumps from center tank to each wing tank; 4 boost pumps (2 active and 2 standby) from wing tank left/right to engine left/right; 1 boost pump from center tank to APU
Hydraulic power supply system (HPSS)	2 networks (green, yellow), 1 EDP green at each engine; 1 EDP yellow at each engine; 1 EMP green for backup; 1 EMP yellow for backup; system pressure: 3000 psi
Pneumatic power supply system (PPSS)	1 low-pressure and 1 high-pressure bleed air station and 1 precooler at each engine; pressure regulation valves, cross-flow valve to connect left and right wing sides; ducts from both engines and the APU to both ECS packs and to the WIPS duct interfaces at both wing sides (cf. Figure 10)
Electric power supply system (EPSS)	Distributed architecture, details see Table 6
Other	Integrated modular avionics, instruments and navigation, communications, auto flight, fire protection, oxygen, water/waste, inert gas
	asile, asile ingin, in a protestion, oxygon, nator, nato, mort gue

Table 6 provides a comprehensive description of the EPSS. Furthermore, the DLR-F25 incorporates integrated modular avionics and a non-halon fire protection system. With regard to the remaining systems listed in Table 5, it can be stated that there are no significant changes for the DLR-F25 in comparison to state-of-the-art technology. The environmental control system and the ice protection system are supplied with engine bleed air. The actuation of the landing gear and cargo doors is fully hydraulic. Regarding the fuel system, the DLR-F25 features one center tank and one tank in each main wing.

Table 6 – Specifications of the electric power supply system for the DLR-F25

Subsystem	Description
Networks	E1 and E2, each with a voltage level of 400/230 VAC at variable frequency; 2 networks with a voltage level of 28 VDC
Power genera- tion	1 variable frequency generator (VFG) with 100 kVA at each engine (E1 generator left and E2 generator right); 1 AC VFG (supplying E1 and E2) with 100 kVA at APU; 1 AC VFG (supplying E1 and E2) with 10 kVA at ram air turbine
Power storage	2 Li-Ion batteries with a voltage level of 24 VDC and a capacity of 50 Ah each (both provide 10 kVA for approx. 15 minutes)
Power trans- formation	2 transformer rectifier units (TRU) with 5.5 kVA each for normal operation (transform 400/230 VAC to 28 VDC); 1 TRU with 5.5 kVA for emergency operation (transforms 400/230 VAC to 28 VDC); 1 static inverter with 2 kVA (transforms 28 VDC to 400/230 VAC)
Power management and distribution	2 primary electric power distribution centers (PEPDC) below cockpit; 2 secondary electric power distribution centers (SEPDC) below cockpit; 6 secondary power distribution boxes (SPDB) in cabin; 2 SPDBs in cargo compartment
Ground power	1 connector with 90 kVA

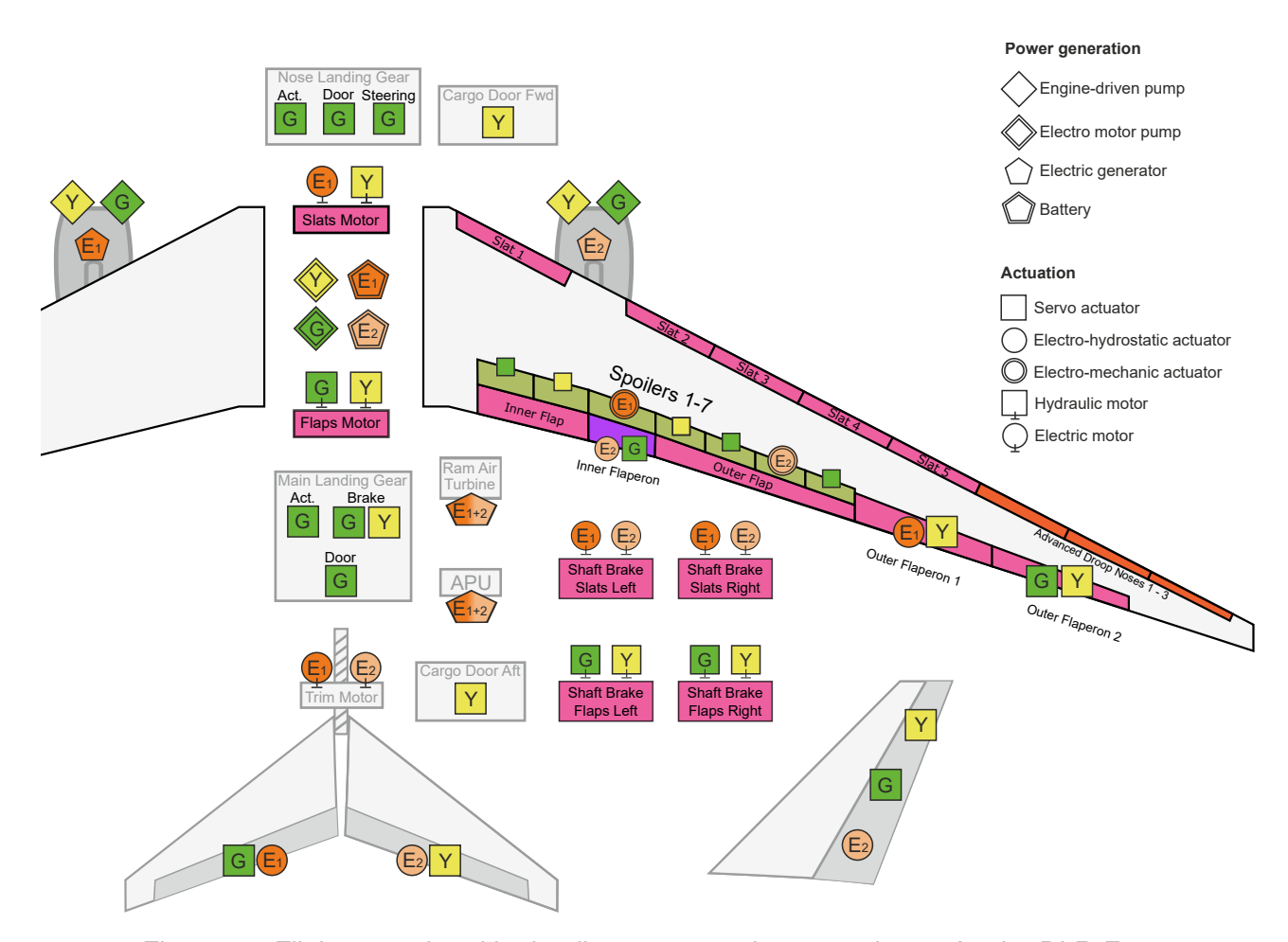


Figure 9 - Flight control and hydraulic power supply system layout for the DLR-F25

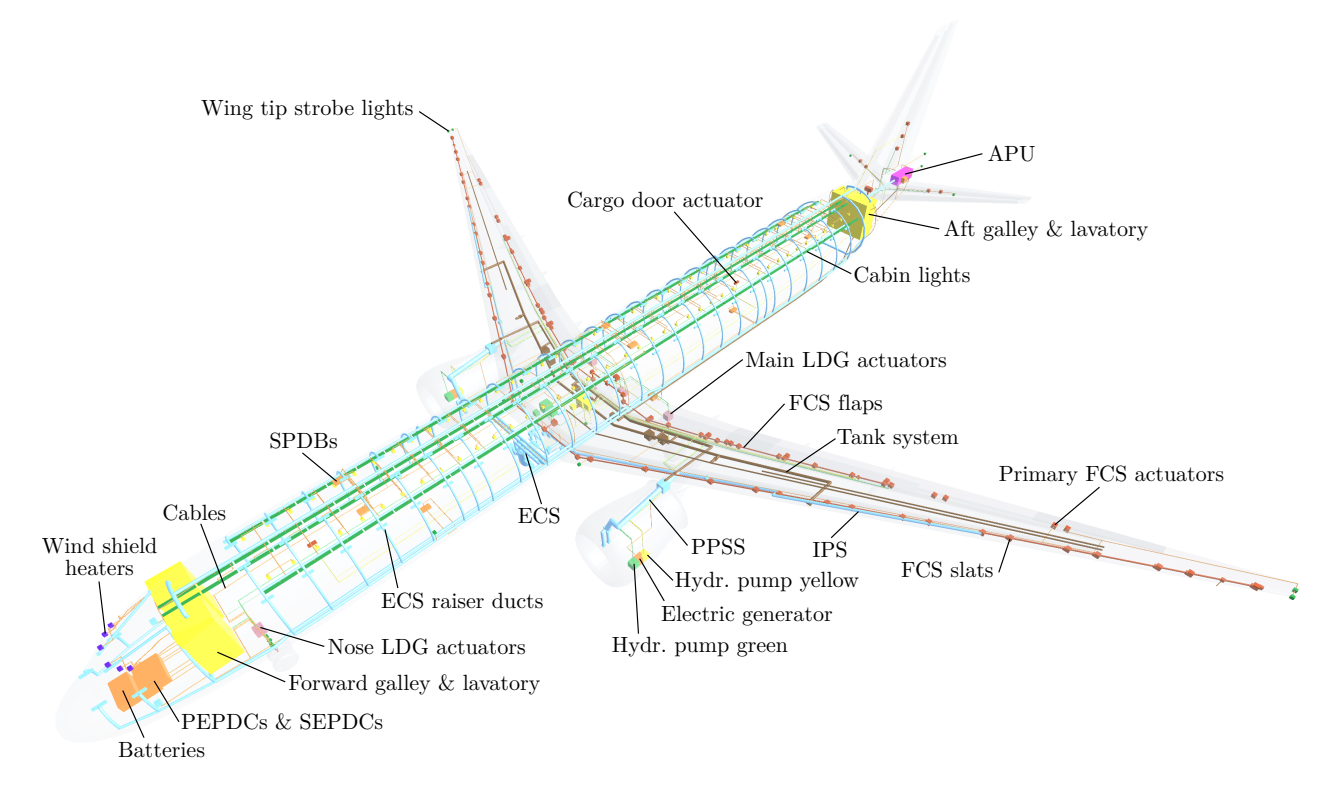


Figure 10 – Topology of the overall on-board systems architecture of the DLR-F25

4.2 Systems Architecture Sizing Results

With regard to the conceptual design of the aircraft on-board systems for the DLR-F25, the OSD framework, as outlined in Section 2.3, is applied. The initial step is the generation of the topology. The result of the OBS topology generation for the DLR-F25 is depicted in Figure 10.

The subsequent sizing and simulation procedure within the OSD framework estimates, among other things, the mass at component and system level, the center of gravity at system level, and the shaft and bleed air power off-take demands of the overall systems architecture throughout the reference mission. With regard to mass, Figure 11 provides a mass breakdown at system level for the DLR-F25 in relation to the D239's state-of-the-art OBS architecture. For the sake of clarity, it should be noted that the breakdown does not include cabin equipment and furnishings. A detailed mass breakdown for the DLR-F25 is presented in Figure 24, which includes the total OBS mass.

The discrepancy in system masses between the D239 and the DLR-F25, as illustrated in Figure 11, is primarily attributable to the implementation of a more electric OBS architecture for the DLR-F25. For the sizing of the ECS, an increased passenger comfort is assumed, which can be achieved through an increased air exchange rate within the cabin. This results in a more powerful pack, which in turn leads to a higher mass, compared to the state-of-the-art technology assumed for the D239. The electrification of the FCS for the DLR-F25 based on the D239 architecture results in an increase in the mass of the FCS. Concurrently, the mass of the HPSS is reduced, as one of the hydraulic networks is no longer required for the DLR-F25. While the electrified FCS tends to elevate the electrical power demand of the system architecture, the mass of the EPSS for the DLR-F25 is less than that of the D239. This can be attributed to the distributed EPSS architecture and the elevated voltage level, which permits the selection of smaller cable cross-sections. As the integrated modular avionic is included in the category of other systems and the number of computers and cables increases with its installation, the mass of the other systems for the F25 is also higher than for the D239.

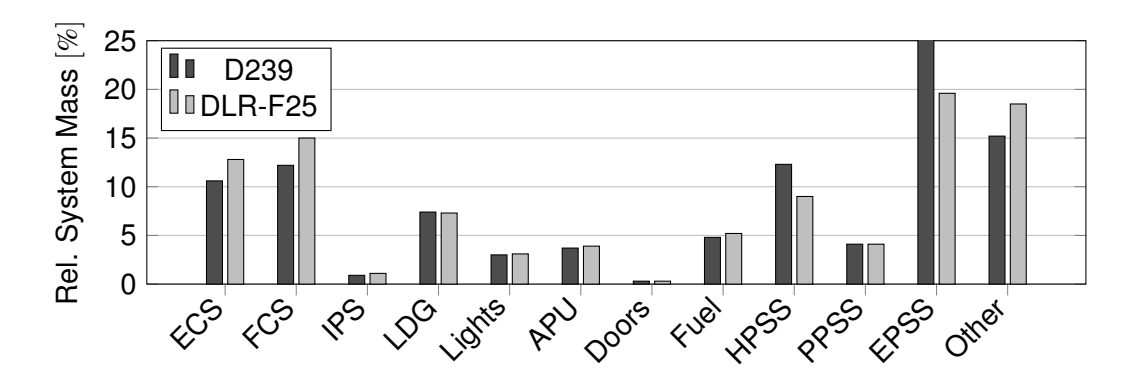


Figure 11 – Preliminary on-board systems mass results for the DLR-F25 in comparison to the D239

The bleed air mass flow required by one engine to supply the systems with pneumatic power throughout the mission is depicted in Figure 12. Peak values of $0.9\,\mathrm{kg/s}$ per engine are estimated for nominal operating conditions for the DLR-F25. The peak values represent the operation of the ECS and, in addition, the IPS during both climb and descent. During the cruise phase, it is estimated that a bleed air mass flow of $0.425\,\mathrm{kg/s}$ per engine is required as a result of continuous ECS operation.

Regarding the shaft power off-takes for one engine as depicted in Figure 13, a peak value of $80 \, \mathrm{kW}$ per engine is observed for the DLR-F25 under nominal operating conditions. This peak value is reached mid-cruise, as galley operation is assumed at this point. The electric and hydraulic power base consumption during cruise is estimated to be around $55 \, \mathrm{kW}$. The peak observed at the outset of the flight mission is largely attributable to the augmented power demand of the fuel pumps.

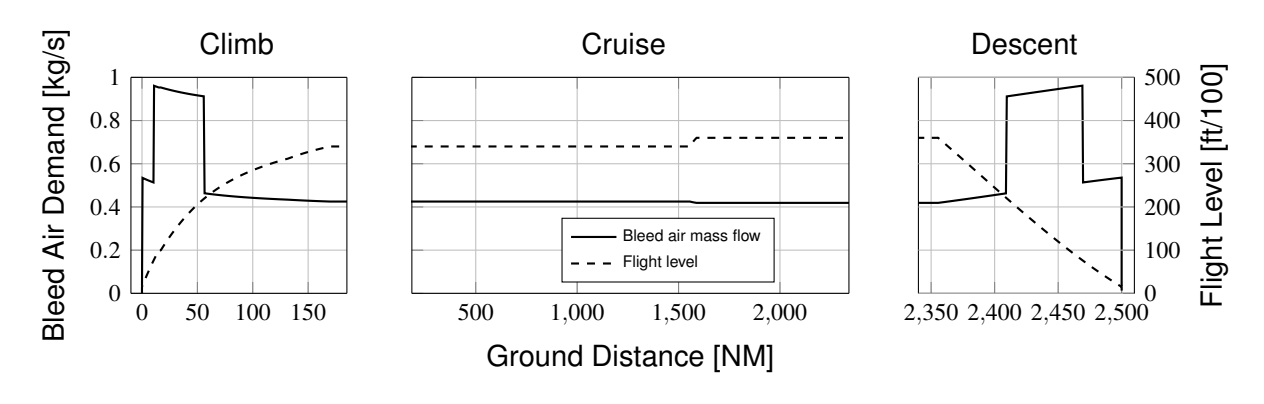


Figure 12 – Bleed air requirements for the DLR-F25 for one engine

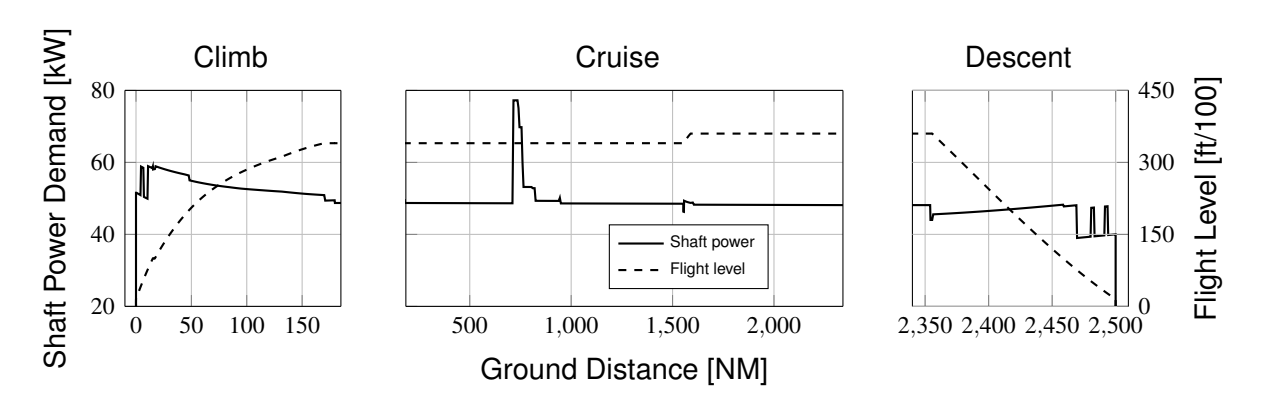


Figure 13 – Shaft power requirements for the DLR-F25 for one engine

In summary, the DLR-F25 concept aircraft comprises an electrified on-board systems architecture. Thus, a research baseline with entry into service in 2035 is available for conducting future trade studies.

5. Aircraft Design and Performance of the DLR-F25

The reference aircraft for the VirEnfREI project is the Airbus A321neo [23]. As the initial step, the reference aircraft will be redesigned and calibrated within the same aircraft design environment as used for the DLR-F25 configuration to establish a consistent design. The D239 is therefore redesigned and calibrated as a similar aircraft to the Airbus A321neo in terms of geometry, design masses and performance based on publicly available data [23, 25]. The design process of the DLR-F25 configuration is then initiated and the defined technology assumptions are applied.



Figure 14 – Aircraft design process from the A321neo reference aircraft [23] to the D239 as the SMR representative aircraft to the DLR-F25 configuration.

5.1 Technology Integration

The particular focus of the DLR-F25 design is on the integration of the advanced very high aspect wing that was derived during the first year of the VirEnfREI project as an initial shape design, see Figure 15. Compared to previous studies, the 36m wing span gate limit has been relaxed to identify the potential of an unconstrained span while considering the integration of a foldable wing tip device similar to the Boeing 777X. The difference with this design is that the movable devices are also placed outside the folding mechanism to significantly increase the span. The aerodynamic performance of the wing is modelled and derived at the overall aircraft design level described in Chapter 2 and will be designed in detail in scope of the VirEnfREI [28, 29] and UP Wing projects [30]. The wing planform was derived to study the integration of the movable layout and high lift devices along with the aerodynamic twist and airfoil design. As part of the UP Wing project, the initial layout of the primary and secondary flight control surfaces was revised to achieve the maximum lift coefficient necessary to meet the approach speed requirements with the predefined wing geometry, area and adaptive dropped hinge trailing edge architecture [31].

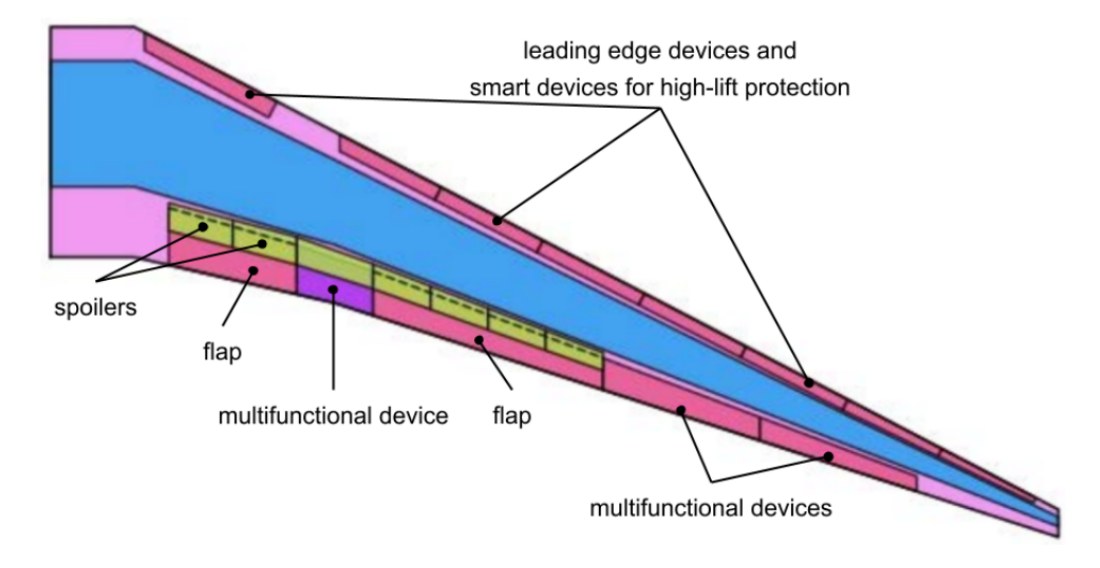


Figure 15 – Movable layout and geometry of the very high aspect ratio wing of the DLR-F25 retrieved from [30]

The detailed design is described by Eberle et. al [30]. The initial structure mass has been assessed by analytical structural sizing performed in the VirEnfREI project and will be sized in detail using aero-structural coupled wing design including profiles, masses, lift distribution and performance calculation. For the iterative design process, the structure will be resized while keeping the geometry constant for consistency due to the detailed analysis to be performed in various research projects. The fuselage geometry is kept consistent with the reference aircraft in terms of cross section, overall height and width, and cabin layout. The structure is resized with regard to the wing integration and the estimated flight, gust and landing loads. Due to the slender wing root chord, the aspect ratio and sweep of the wing and the overall centre of gravity, a wing-mounted landing gear integration is not feasible and therefore the landing gear is attached to the fuselage. The geometry of the attachment points, the associated loads and structural reinforcements are considered in the structural design of the fuselage and in the aerodynamic design of the belly fairing.

5.2 Thrust Requirements

During the iterative aircraft design process, the thrust requirements are derived for the detailed engine design. For the end of field requirement, low speed performance calculations are performed as depicted in Figure 16 to derive the thrust requirement based on a balance field length analysis.

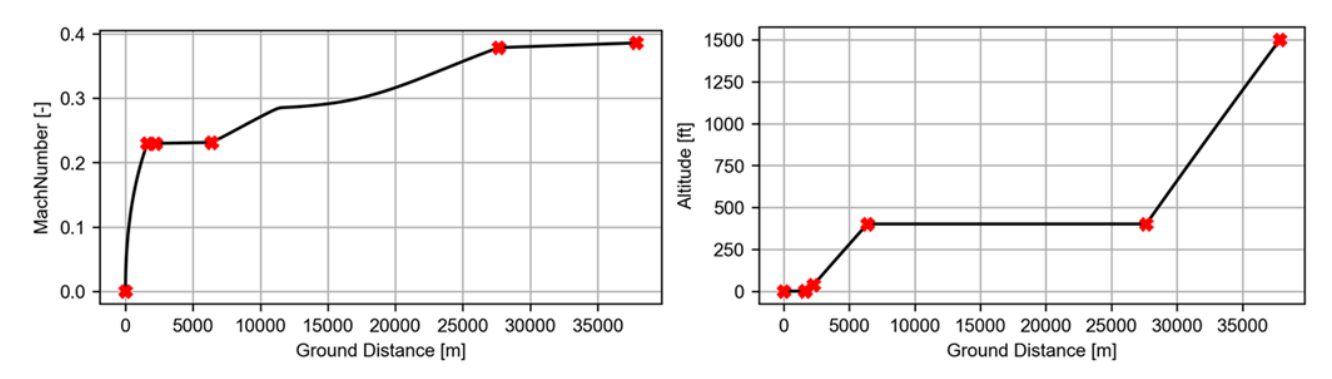


Figure 16 – Low speed performance calculation results of Mach number and altitude over ground distance for thrust requirement definition

The take-off condition is defined as sea level static thrust at maximum take-off mass (MTOM) and is calculated using the thrust lapse. For the remaining flight conditions, the equation of motion is solved with the boundary conditions mentioned hereafter. At the end of field, the aircraft is on the ground at lift-off speed, in take-off configuration and approximately at MTOM. The second segment is also defined at approximately MTOM in take-off configuration with the landing gear retracted at the initial climb speed, no ground effects considered, critical engine inoperative and at least a climb gradient greater than 2.4% at 35ft. Top of climb (TOC) is defined at flight level 330, the block fuel optimum initial cruise altitude and an available rate of climb of 300 ft/min or greater. Top of climb +2000ft defines a thrust requirement with an additional margin of 2000ft above the TOC condition for wind gradients and step climb capability to reach the optimum altitude during the cruise segment. Mid cruise defines the cruise condition at flight level 350 in the middle of the flight segment. The design and evaluation mission trajectories are plotted in Figure 17 and in detail in Figure 26. The 800nm evaluation mission is selected as the most representative mission for the short-medium range market and is used for the technology assessment.

The thrust requirements for all design conditions of the final design iteration are summarised in Table 7. The power and bleed air off-takes are derived from the detailed on-board system design. For take-off, end of field and second segment, the off-takes are defined in the critical one-engine inoperative condition while TOC, TOC +200ft and mid cruise are defined in typical operation at these flight phases.

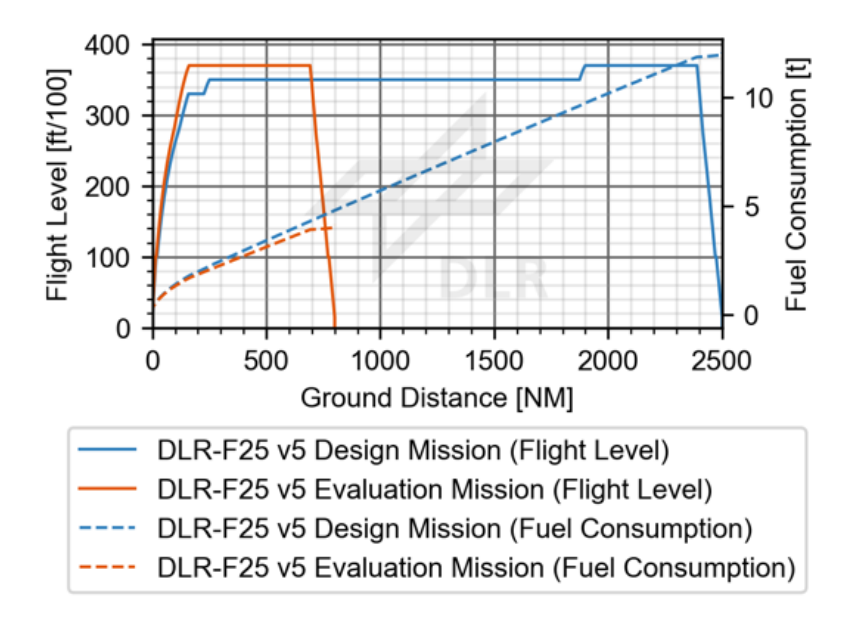


Figure 17 – Flight trajectories for the design and evaluation mission of the DLR-F25

Table 7 – Thrust requirements for take-off, end of field, 2nd segment, top of climb and mid cruise condition for the engine design of the DLR-F25 configuration

Parameter	Unit	Take-	End of	2nd	TOC	TOC	Mid
		Off	Field	Seg.		+2000ft	Cruise
Delta Temp. ISA	[K]	15.0	15.0	15.0	10.0	10.0	0.0
Mach-Number	[-]	0.0	0.23	0.24	0.76	0.76	0.78
Altitude	[Ft]	0.0	0.0	400	33000	35000	35000
Engine Rating	[-]	MTO	MTO	MTO	MCL	MCL	MCR
Thrust	[kN]	124.7	86.9	76.1	22.4	23.0	19.1
Shaft-Power Offtakes	[kW]	95	95	95	50	50	50
Bleed Air Offtakes	[kg/s]	0.0	0.0	0.0	0.425	0.425	0.425

5.3 Technology Assessment

In order to identify the impact of each technology applied at aircraft level during the design process, a stepwise approach was taken to derive the overall performance of the DLR-F25 configuration compared to the D239 reference aircraft described in Figure 18 on the 800nm evaluation mission selected as the most representative mission for the short-medium range market. At each step, a complete aircraft design loop is performed, iterating the geometry of all affected components, aerodynamic characteristics and masses until convergence is achieved. For example, the engine is rescaled for the updated thrust requirements, and the wing area is adjusted at each step based on fuel volume, take-off performance and approach speed requirements, among other aircraft components and characteristics.

In the first step, only the technology assumptions for the fuselage and tail, introduced in Table 2, are applied. Therefore, the aircraft is resized starting from the reference calibration. Due to the relatively minor mass savings associated with the applied technology factors, a minor block fuel saving of about 1% is identified. This already includes snowball effects, improvements due to the resizing of the aircraft based on mass savings and performance improvements, in addition to the mass savings of the fuselage and tailplane structure.

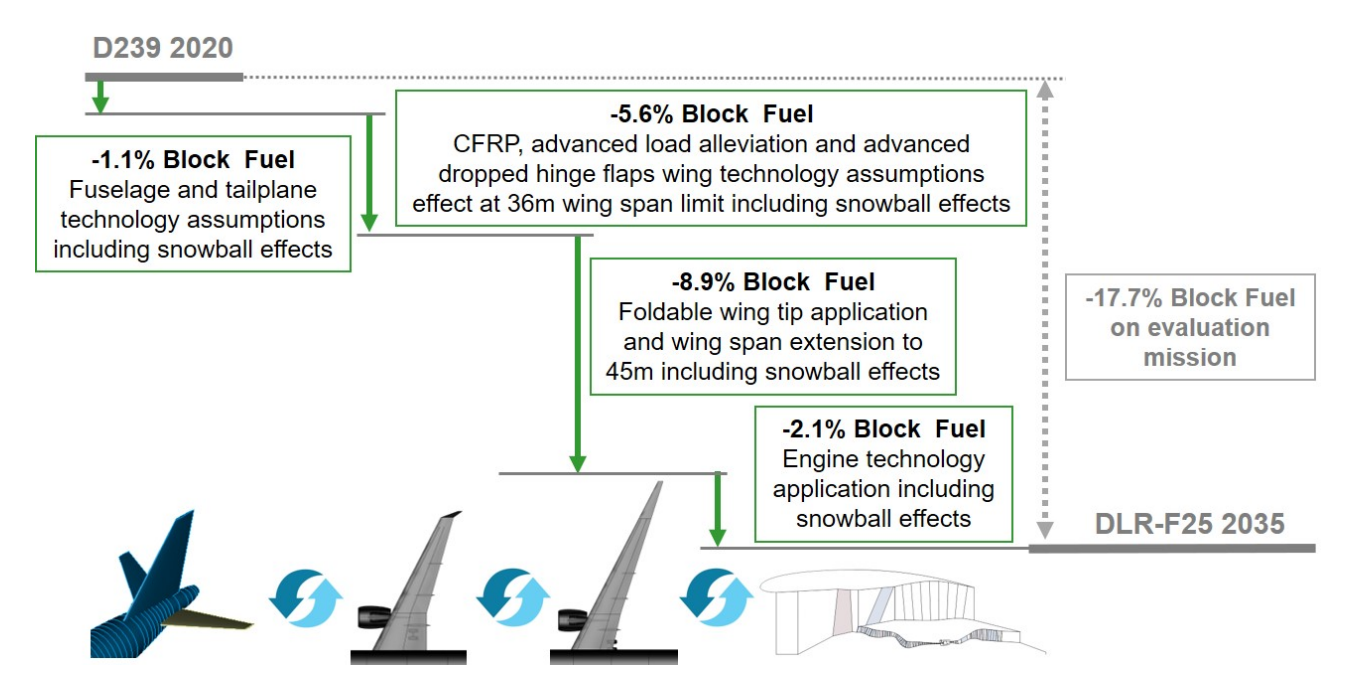


Figure 18 – DLR-F25 stepwise technology assessment on aircraft level for the evaluation mission of 800nm

The second step is to integrate all the wing technologies discussed, with the exception of the folding wingtip mechanism and its associated span extension. This is done to isolate and highlight the impact of this technology in particular at the next step. Thus, an additional 5.6 % block fuel saving is achieved by significantly reducing the structural mass of the wing and thereby increasing the aspect ratio of the wing and the aerodynamic efficiency by reducing the wing area and the corresponding friction and induced drag accordingly, while maintaining the 36m span limit.

Then the folding wingtip and span extension are introduced, including the mass penalty for system mass and structural strengthening of the wing. By extending the wingspan from 36m to 45m for a comparable wing area, the aspect ratio of the wing is greatly increased and the induced drag of the aircraft is significantly reduced. This has the most significant impact on the block fuel saving potential compared to the reference aircraft, accounting for almost half of the total improvement.

The final step is to integrate the detailed engine performance, geometry and mass into the aircraft design. As the nacelle outside diameter, overall length and mass of the engine are comparable to those of the reference engine, no major adjustments are required at aircraft level. Due to the superior overall efficiency of the engine, an additional 2.1% block fuel improvement can be achieved, resulting in a total block fuel improvement of 17.7% over the reference aircraft. The engine integration benefit achieved is less than the overall 4% TSFC improvement described in Table 2 and Table 8. The explanation for this discrepancy is that the engine for the high aspect ratio wing is a downsized version of the reference engine based on the derived thrust requirements identified in this design iteration. Therefore, the increased diameter and mass of the 2035 engine offset the improvement in TSFC over the previous design step for this incremental application of technologies where part of the engine improvement potential is already accounted for.

5.4 Aircraft Characteristics of the DLR-F25

The DLR-F25 configuration is the result of inputs from various projects and detailed studies, and will be further investigated as the projects progress. A summary of the current status of the aircraft configuration and its key characteristics is presented in Table 8 and compared with the D239 reference aircraft as the result of the overall aircraft design study. Figure 19 gives a first impression of the aircraft configuration by providing a three-view of the DLR-F25 configuration. The Appendix contains the detailed wing planform definition in Figure 15, the wing and tailplane characteristics in Figure 22, the aerodynamic characteristics in Figure 23, the detailed mass breakdown in Figure 24 and the payload-range characteristic in Figure 25 of the DLR-F25.

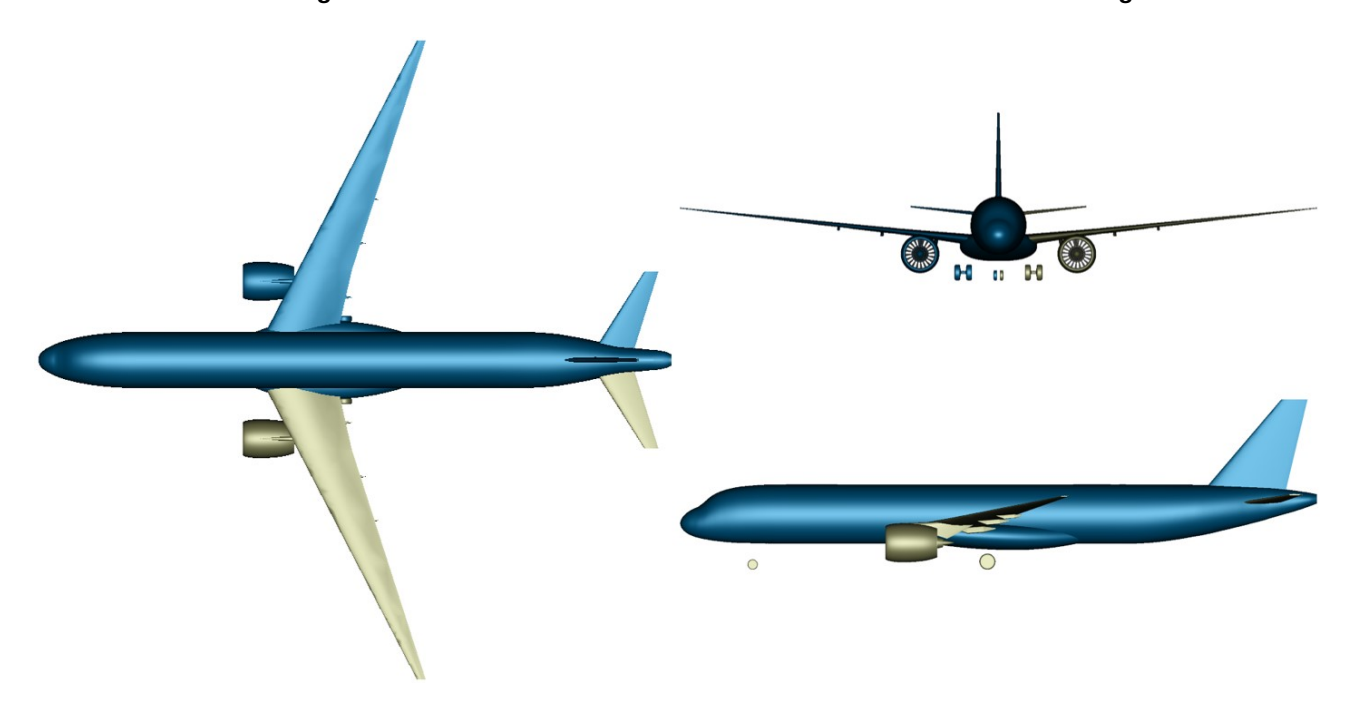


Figure 19 – Three view of the DLR-F25 configuration

Table 8 – Comparison of the DLR-F25 aircraft characteristics to the D239 reference aircraft

Key Sizing Parameters		D239	DLR-F25
W/S=MTOM/Sref	[kg/m2]	719.8	658.6
T/W=SLST/MTOM	[-]	0.319	0.296
Masses			
Max. Take-Off Mass	[t]	93.5	85.7
Max. Landing Mass	[t]	79.2	74.2
Max. Zero Fuel Mass	[t]	75.6	71.3
Operating Empty Mass	[t]	50.6	46.3
Max. Fuel Mass	[t]	18.4	16.7
Block Fuel (Design Range)	[t]	15.0	12.1
Block Fuel (Evaluation Range)	[t]	5.0	4.1
Geometry			
Wing Span	[m]	36	45
Wing Aspect Ratio	[-]	9.9	15.6
Wing MAC	[m]	4.30	3.54
Wing Ref. Area	[m2]	129.9	130.1
Propulsion			
Equivalent static thrust (Sea-level/ISA)	[kN]	147.3	124.5
TSFC cruise average (800nm)	[kg/s/kN]	0.0149	0.0143
Aerodynamic			
cL cruise (800nm)	[-]	0.581	0.593
L/D cruise average (800nm)	[-]	17.5	19.5
cL max TO	[-]	2.4	2.3
cL max LDG	[-]	3.05	2.845

Figure 20 illustrates the main differences between the D239 (shown in green) and DLR-F25 (shown in blue) aircraft configurations in a superimposed top view, highlighting the difference in the aspect ratio and span of the wings. It can be noted that the fuselage is kept constant between the two configurations, while the aspect ratio of the horizontal stabilizer has been adapted to the higher aspect ratio of the wing and has been reduced in area as a result of the slightly increased lever arm and reduced mean aerodynamic chord of the wing, while maintaining the same volume coefficient. The increased lever arm is the result of shifting the wing position forward to maintain the overall static margin of the reference configuration with respect to changes in wing and engine position and mass. As a result, the main landing gear can no longer be attached to the wing and must be attached to the fuselage. Therefore, the belly fairing must be sized to accommodate the landing gear.

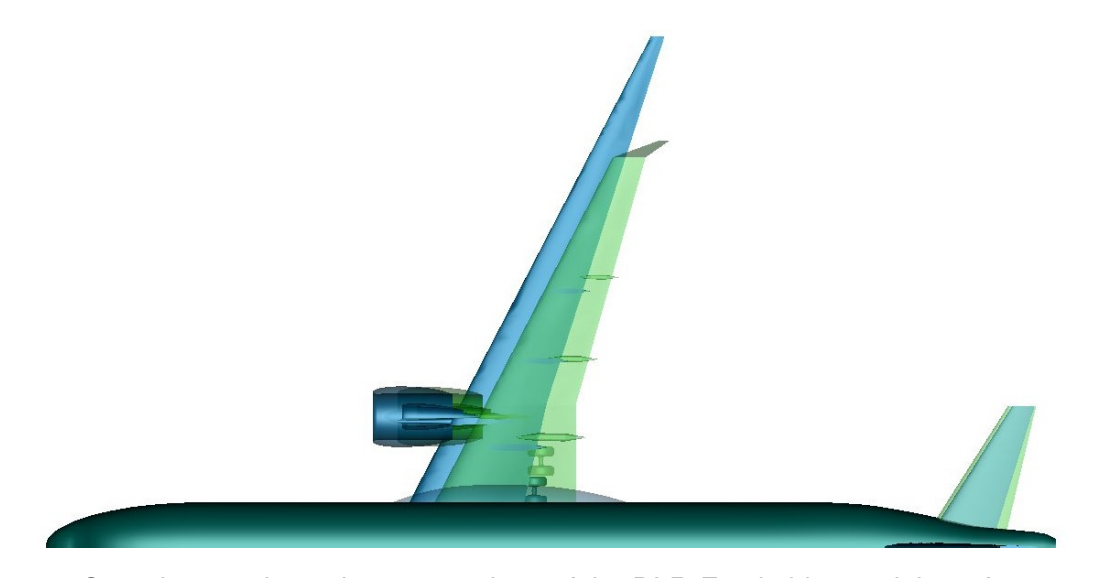


Figure 20 – Superimposed top view comparison of the DLR-F25 in blue and the reference aircraft D239 in green

As derived in Chapter 5.3, the DLR-F25 offers a 17.7% block fuel advantage over the reference aircraft in the typical operational scenario of the evaluation mission, with the major contribution coming from the advanced wing technology. With a lower maximum lift coefficient in landing configuration at the same approach speed for the DLR-F25 due to a different movable layout and different trailing edge devices, the wing area of both aircraft is very similar at 129 square metres for the D239 and 130 square metres for the DLR-F25. The improvement in lift over drag can therefore be directly compared, and an improvement of 13% is observed for the DLR-F25 at mid cruise condition. This advantage is mainly due to the reduced induced drag resulting from the very high aspect ratio of 15.6 compared to 9.9 for the D239. Combined with the structural mass savings from the advanced load alleviation system, the use of CFRP and active flutter suppression, the wing technology accounts for approximately 14.5% of the 17.7% block fuel saving. The structural mass savings and aerodynamic efficiency improvements are derived through analytical methods. A detailed analysis will be carried out to verify the results derived from the overall aircraft design by applying the Cybermatrix approach [3] developed at DLR for multidisciplinary design optimization in the VirEnfREI project and the detailed wing design to be performed in the scope of the Clean Aviation UP Wing project.

5.5 Sensitivities Study

To assess the impact of technologies on overall aircraft performance before they are integrated into the aircraft design, sensitivities can be used to roughly estimate the impact at the overall aircraft level. Sensitivities are trade studies that calculate the impact of a given input variable at aircraft level, including snowball effects by resizing the aircraft. This involves reassessing geometry, engine and aerodynamic performance, and mission performance. Based on the sensitivities, component level trade studies and optimisations, such as engine design studies, can be carried out to a certain extent without aircraft level integration if the overall aircraft configuration is not affected. Sensitivities are

calculated for small variations where the influence is expected to be linear. Therefore, the effects of thrust specific fuel consumption (TSFC), mass and drag coefficients on block fuel (FB) are studied through the aircraft design process. The change in TSFC is applied to the engine performance by an appropriate factor. To estimate the effect of mass (M), an additional miscellaneous mass is added to the centre of gravity of the operating empty mass so as not to affect the overall configuration, and the drag coefficients (dc) are applied as a delta to the zero lift drag coefficient of the aircraft at mid cruise. The reference wing area is 130m². The parameter variations presented are therefore independent of any specific technology development. The following sensitivities are derived for the DLR-F25 configuration:

Sensitivities for the 2500nm design mission:

$$\frac{\partial FB}{\partial TSFC} = 1.33 \frac{\%}{\%} \qquad \frac{\partial FB}{\partial M} = 2.04 \frac{\%}{t} \qquad \frac{\partial FB}{\partial dc} = 3.31 \frac{\%}{10 dc}$$
 (2)

Sensitivities for the 800nm evaluation mission:

$$\frac{\partial FB}{\partial TSFC} = 1.16 \frac{\%}{\%} \qquad \frac{\partial FB}{\partial M} = 1.90 \frac{\%}{t} \qquad \frac{\partial FB}{\partial dc} = 3.15 \frac{\%}{10 dc}$$
(3)

6. Conclusion

The DLR-F25 configuration is intended to be the starting point for various research projects within Clean Aviation, the German funded research programme LuFo and DLR internal projects. To establish the DLR-F25 as a common research baseline, a consistent definition of requirements, design process, design rationale and aircraft characteristics is required. Therefore, the aircraft and engine design process, architecture and characteristics, on-board systems architecture, TLARs and technology assumptions of the DLR-F25 research baseline aircraft are introduced and documented. Based on the derived sensitivities of drag reduction, mass savings and engine efficiency improvement, the impact of additional technologies and advancements can be estimated already at the component level, thus providing guidance for the evaluation of technologies not yet integrated.

With the established level of detail, the DLR-F25 provides an ideal starting point for additional design and trade studies as a meaningful point of comparison and assessment of a conventional aircraft configuration for the short-medium range market segment with a technology level for 2035. The research baseline will be used to assess the integration of alternative propulsion architectures, such as the open fan engine design, and to evaluate different aircraft configurations, such as the truss braced wing concept in the frame of LuFo projects. The DLR-F25 system architecture will serve as an agreed baseline for future trade studies, particularly in relation to the hybrid electric turbofan designs and hydrogen powered aircraft variants being considered in the scope of Clean Aviation and the ACAP project.

Overall aircraft design studies with inputs from high-fidelity detailed design indicate a block fuel reduction of 17.7% compared to the D239, representing the 2020 state-of-the-art aircraft on the 800nm typical mission for the short-medium range market segment. When detailing the impact of the integrated technologies, the wing span extension, which circumvents the 36m gate limit through a foldable wing tip device, has the most significant impact on the overall block fuel saving. The very high aspect ratio is achieved through the use of CFRP, advanced load alleviation and active flutter suppression, while the potential remains to be proven through detailed aero-structure coupled design studies. While significant advances in aircraft design over the last few decades have been dominated by engine improvements, the wing technologies introduced, and in particular the wing span extension, have the potential to outperform engine improvements and deliver significant efficiency gains in the next generation of aircraft.

As further improvements are required to meet the European Green Deal targets, the DLR-F25 is well placed to investigate and demonstrate further improvements through the integration of additional technologies on a detailed aircraft configuration.

7. Contact Author Email Address

Sebastian Wöhler, German Aerospace Center (DLR), Institute of System Architectures in Aeronautics, Hamburg, Germany mailto: sebastian.woehler@dlr.de

8. Copyright Statement

The authors confirm that they, and/or their company or organization, hold copyright on all of the original material included in this paper. The authors also confirm that they have obtained permission, from the copyright holder of any third-party material included in this paper, to publish it as part of their paper. The authors confirm that they give permission, or have obtained permission from the copyright holder of this paper, for the publication and distribution of this paper as part of the ICAS proceedings or as individual off-prints from the proceedings.

9. Acknowledgment

The development of the DLR-F25 configuration is funded by the German Federal Ministry for Economic Affairs and Climate Action (BMWK) as part of the LuFo VI-2 project VirEnfREI (funding reference: 20X2106B).

Supported by:



on the basis of a decision by the German Bundestag

The on-board system design is funded by the European Community's Clean Aviation programme in the frame of the the SMR ACAP project (SMR aircraft architecture and technology integration project). This project has received funding from the European Union's Horizon Europe research and innovation program under Grant Agreement number 101101955. Views and opinions expressed are however those of the authors only and do not necessarily reflect those of the European Union or the Aviation Joint Undertaking. Neither the European Union nor the granting authority can be held responsible for them.





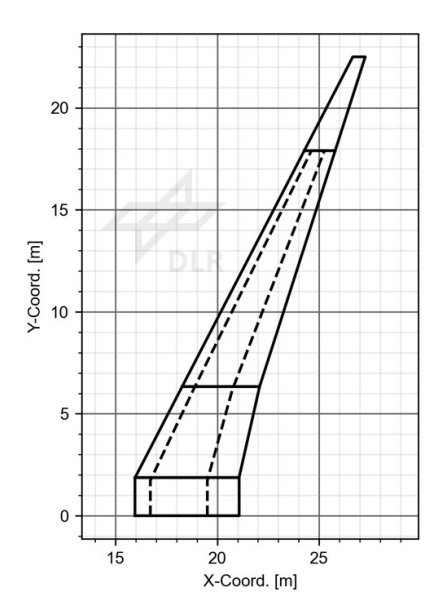
References

- [1] European Commission, "COMMUNICATION FROM THE COMMISSION The European Green Deal," communication and roadmap on the european green deal, European Commission, Brussels, Belgium, May 2019. COM(2019) 640 final.
- [2] German Aerospace Center, "TOWARDS ZERO-EMISSION AVIATION How DLR's Aviation Research Strategy supports the European Green Deal 2050," booklet, DLR, Cologne, Germany, 2021.
- [3] C. Ilic, A. Merle, M. Abu-Zurayk, S. Goertz, M. Leitner, Özge Süelözgen, T. Kier, M. Schulze, T. Klimmek, C. Kaiser, D. Quero, A. Schuster, M. Petsch, D. Kohlgrüber, J. Häßy, R. Becker, and S. Gottfried, "Cybermatrix protocol: a novel approach to highly collaborative and computationally intensive multidisciplinary aircraft optimization," in AIAA AVIATION Forum 2020, (Virtual Event), American Institute of Aeronautics and Astronautics, 2020.

- [4] S. Wöhler, G. Atanasov, D. Silberhorn, B. Fröhler, and T. Zill, "Preliminary aircraft design within a multidisciplinary and multifidelity design environment," in *Aerospace Europe Conference 2020*, (Bordeaux, France), 2020.
- [5] B. Boden, J. Flink, N. Först, R. Mischke, K. Schaffert, A. Weinert, A. Wohlan, and A. Schreiber, "Rce: An integration environment for engineering and science," *SoftwareX*, vol. 15, p. 100759, 2021.
- [6] M. Alder, E. Moerland, J. Jepsen, and B. Nagel, ""recent advances in establishing a common language for aircraft design with cpacs," in *Aerospace Europe Conference 2020*, 2020.
- [7] R.-G. Becker, S. Reitenbach, C. Klein, T. Otten, M. Nauroz, and M. Siggel, "An integrated method for propulsion system conceptual design," in *Proceedings of the ASME Turbo Expo: Turbine Technical Conference and Exposition 2015*, (New York, NY), ASME, 2015.
- [8] S. Reitenbach, A. Krumme, T. Behrendt, M. Schnös, T. Schmidt, S. Hönig, R. Mischke, and E. Mörland, "Design and application of a multidisciplinary predesign process for novel engine concepts," *Journal of Engineering for Gas Turbines and Power*, vol. 141, no. 1, 2019.
- [9] S. Reitenbach, M. Vieweg, R. Becker, C. Hollmann, F. Wolters, J. Schmeink, T. Otten, and M. Siggel, "Collaborative aircraft engine preliminary design using a virtual engine platform, part a: Architecture and methodology," in *AIAA Scitech 2020 Forum*, (Reston, Virginia), American Institute of Aeronautics and Astronautics, 01062020.
- [10] J. Häßy and J. Schmeink, "Knowledge-based conceptual design methods for geometry and mass estimation of rubber aero engines," in *ICAS 2022 33rd Congress of the International Council of the Aeronautical Sciences*, (Stockholm, Sweden), 2022.
- [11] J. Häßy and B. Fröhler, The Virtual Propulsion Expert: Application of a Hybrid Surrogate-Based Rubber Engine Model in Aircraft Design.
- [12] J. Häßy, M. Bolemant, and R.-G. Becker, "An Educated Guess Predicting Turbomachinery Efficiencies of Aero Engines During Conceptual Design," vol. Volume 1: Aircraft Engine of *Turbo Expo: Power for Land, Sea, and Air*, p. V001T01A033, 06 2023.
- [13] P. Wehrel, R. Schöffler, C. Grunwitz, F. Carvalho, M. Plohr, J. Häßy, and A. Petersen, "Performance and Emissions Benefits of Cooled Ceramic Matrix Composite Vanes for High-Pressure Turbines," *Journal of Engineering for Gas Turbines and Power*, vol. 145, p. 121016, 10 2023.
- [14] N. Kuelper, J. Broehan, T. Bielsky, and F. Thielecke, "Systems Architecting Assistant (SArA) Enabling A Seamless Process Chain from Requirements to Overall Systems Design," in *33rd Congress of the International Council of the Aeronautical Sciences ICAS*, (Stockholm, Sweden), International Council of the Aeronautical Sciences (ICAS), 2022.
- [15] N. Kuelper, T. Bielsky, J. Broehan, and F. Thielecke, "Model-based framework for data and knowledge-driven systems architecting demonstrated on a hydrogen-powered concept aircraft," in *33rd INCOSE International Symposium IS2023*, INCOSE (International Council on Systems Engineering), 2023.
- [16] N. C. Kuelper, V. Starke, J. Broehan, and F. Thielecke, *Evaluation Metrics for Systems Architecting demonstrated on Cooling System of Hydrogen-Powered Concept Aircraft*.
- [17] N. Kuelper, V. Kriewall, K. Beschorner, and F. Thielecke, "Techmaps technology management for the architecting process of aircraft on-board systems," in *34th Congress of the International Council of the Aeronautical Sciences (ICAS)*, International Council of the Aeronautical Sciences (ICAS), 2024. (submitted for publication).
- [18] T. Bielsky, M. Juenemann, and F. Thielecke, "Parametric Modeling of the Aircraft Electrical Supply System for overall Conceptual Systems Design," in *German Aerospace Congress*, German Society for Aeronautics and Astronautics Lilienthal-Oberth e.V., 2021.
- [19] T. Bielsky, N. Kuelper, and F. Thielecke, "Assessment of an Auto-Routing Method for Topology Generation of Aircraft Power Supply Systems," in *German Aerospace Congress*, (Dresden, Germany), German Society for Aeronautics and Astronautics Lilienthal-Oberth e.V., Sept. 2022. (submitted for publication).
- [20] M. Juenemann, T. Bielsky, V. Kriewall, and F. Thielecke, "Overall Systems Design Method for Evaluation of Electro-Hydraulic Power Supply Concepts for Modern Mid-Range Aircraft," in *American Institute of Aeronautics and Astronautics (AIAA) Aviation Forum*, (Chicago, USA), American Institute of Aeronautics and Astronautics (AIAA), June 2022.
- [21] T. Bielsky, N. Kuelper, and F. Thielecke, "Overall Parametric Design and Integration of On-Board Systems for a Hydrogen-Powered Concept Aircraft," in *Aerospace Europe Conference AEC*, EUCASS-CEAS, 2023.
- [22] The MathWorks, Inc., "System Composer." Matlab Version R2023a, 2023.
- [23] Airbus S.A.S., "A321 aircraft characteristics airport and maintenance planning," manual, Airbus, 31707 Blagnac Cedex, France, 2020. Rev Apr 01/20.

- [24] S. Wöhler, J.-N. Walther, and W. Grimme, "Design and eco-efficiency assessment of a people mover aircraft in comparison to state-of-the-art narrow body aircraft," in *ICAS 2022 33rd Congress of the International Council of the Aeronautical Sciences*, (Stockholm, Sweden), ICAS, 2022.
- [25] EASA, "Type-certificate data sheet no. easa.a.064 for airbus a318-319-320-321," type-certificate, EASA, 2022. Issue 50.
- [26] International Civil Aviation Organization, "Procedures for air navigation services Aircraft Operations, Volume I Flight Procedures," manual, ICAO, Montreal, Canada, 2018.
- [27] International Air Transport Association, "Aircraft Technology Roadmap to 2050," roadmap, IATA, Montreal, Canada, 2019. Ed. By IATA 2019.
- [28] P. Wegener, "Robust cad methodology for cfd optimizations," in *Aerospace Europe Conference 2023*, (Lausanne, Switzerland), EUCASS-CEAS, 2023.
- [29] C. Ilic, P. Wegener, J. R. Bailo, J. Himisch, S. Geisbauer, F. Lange-Schmuckall, and S. Wöhler, "Phased high-fidelity aerodynamic design from scratch of a very high-aspect ratio narrow-body airliner," in *AIAA AVIATION Forum 2024*, (Las Vegas, Nevada), American Institute of Aeronautics and Astronautics, 2024.
- [30] A. Eberle, B. Stefes, and D. Reckzeh, "Clean aviation ultra-performance wing (up wing)," in *AIAA Scitech 2024 Forum*, (Orlando, Florida), American Institute of Aeronautics and Astronautics, 2024.
- [31] D. Reckzeh, "Multifunctional wing moveables: Design of the a350xwb and the way to future concepts," in *ICAS 2014 29th Congress of the International Council of the Aeronautical Sciences*, (St. Petersburg, Russia), 2014.

Appendix



Wing Section	Unit	Center	Root	Kink	Mid	Tip
Position	m	0.00	1.87	6.33	17.90	22.50
Rel. Position	%	0.00	8.30	28.15	79.56	100.00
Chord	m	5.10	5.10	3.80	1.52	0.61
1/4 Chord Sweep	deg	0.00	0.00	24.02	25.13	25.13
LE Sweep	deg	0.00	0.00	27.40	27.40	27.40
TE Sweep	deg	0.00	0.00	12.80	17.80	17.80
Dihedral	deg	0.00	0.00	8.30	6.40	6.40
Thickness Ratio	%	15.30	15.30	11.60	11.00	11.00
Rel. Spar Position						
Front Spar	%	14.70	14.70	16.40	23.10	27.10
Rear Spar	%	69.50	69.50	66.10	65.40	61.90

Figure 21 – Geometric and structural definition of the DLR-F25 wing planform

Parameter	Unit	Wing	HTP	VTP
Reference Area	m^2	130.09	24.83	23.80
Span	m	45.00	12.41	6.31
Aspect Ratio	-	15.57	6.20	1.68
Taper Ratio	-	0.12	0.33	0.32
Mean Aerodynamic Chord	m	3.54	2.17	4.10
Avg. 1/4 Chord Sweep	deg	25.04	28.85	35.00
Avg. Dihedral	deg	7.15	6.00) -
Lever Arm	m	-	20.65	19.75
Volume Coefficient	-	-	1.1150	0.0803

Figure 22 – Geometric characteristics of wing and tailplane of the DLR-F25

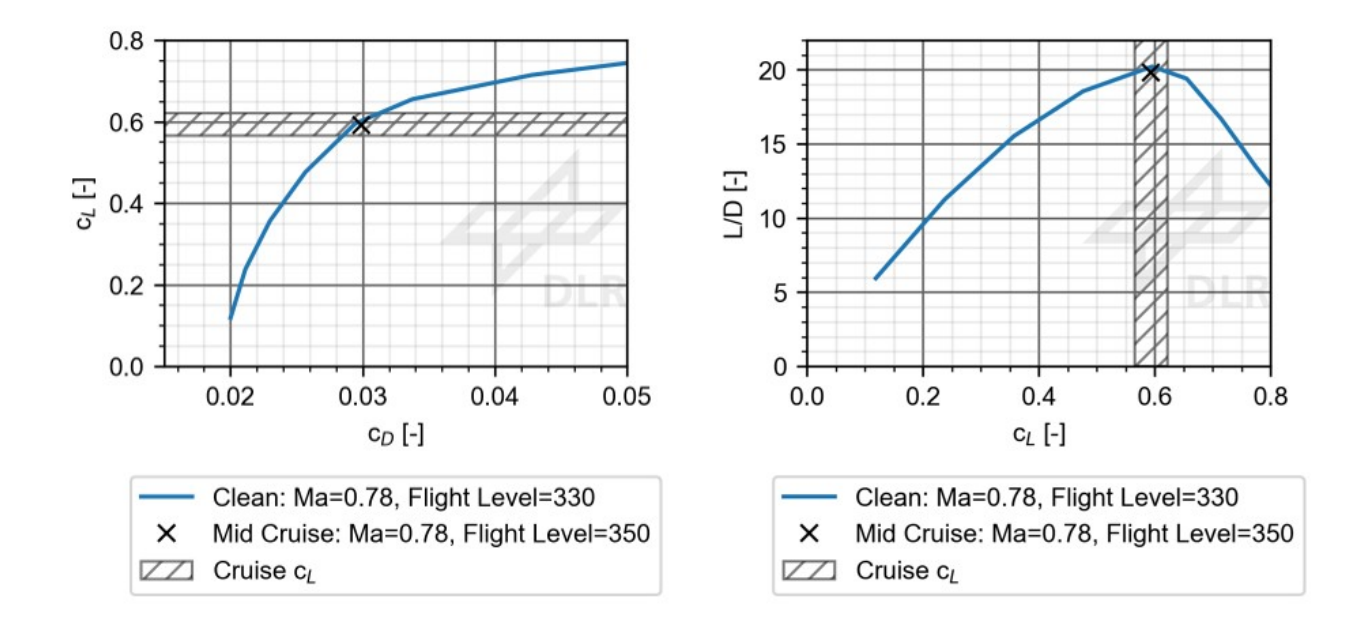
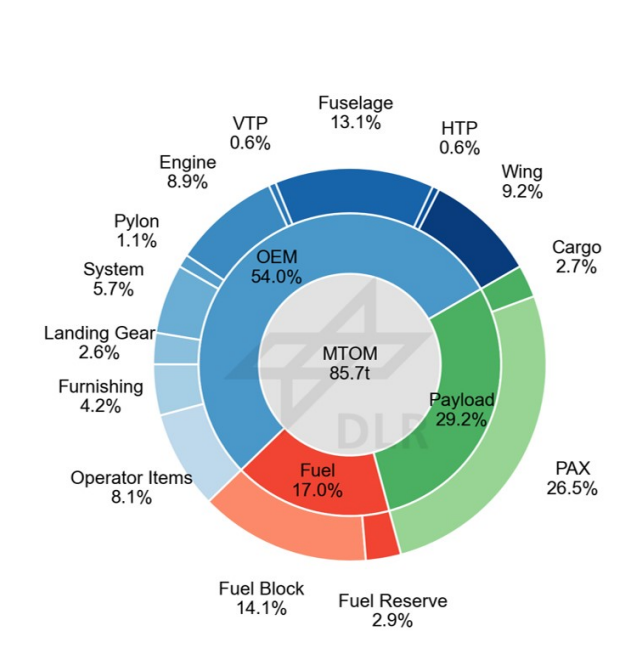


Figure 23 – Aerodynamic characteristics of the mid cruise aerodynamic polar of the DLR-F25



Component	Mass [kg]	x-Pos [m]
Wing	7866	21.08
Fuselage Structure	11261	20.03
НТР	480	41.06
VTP	498	41.11
Pylons	920	18.16
Power Units	7591	16.62
Main Gear	1842	21.48
Nose Gear	370	5.07
Systems	4910	15.8
Furnishings	3600	20.75
Manufacturer Empty Mass (MEM)	39337	-
Operating Items	6934	-
Operating Empty Mass (OEM)	46271	19.71
Maximum Payload	25000	20.75
Maximum Fuel	16725	19.02
Maximum Zero-Fuel Mass (MZFM)	71271	-
Maximum Landing Mass (MLM)	74170	=
Maximum Take-Off Mass (MTOM)	85688	19.94

Figure 24 - Detailed mass breakdown and centre of gravity of the DLR-F25

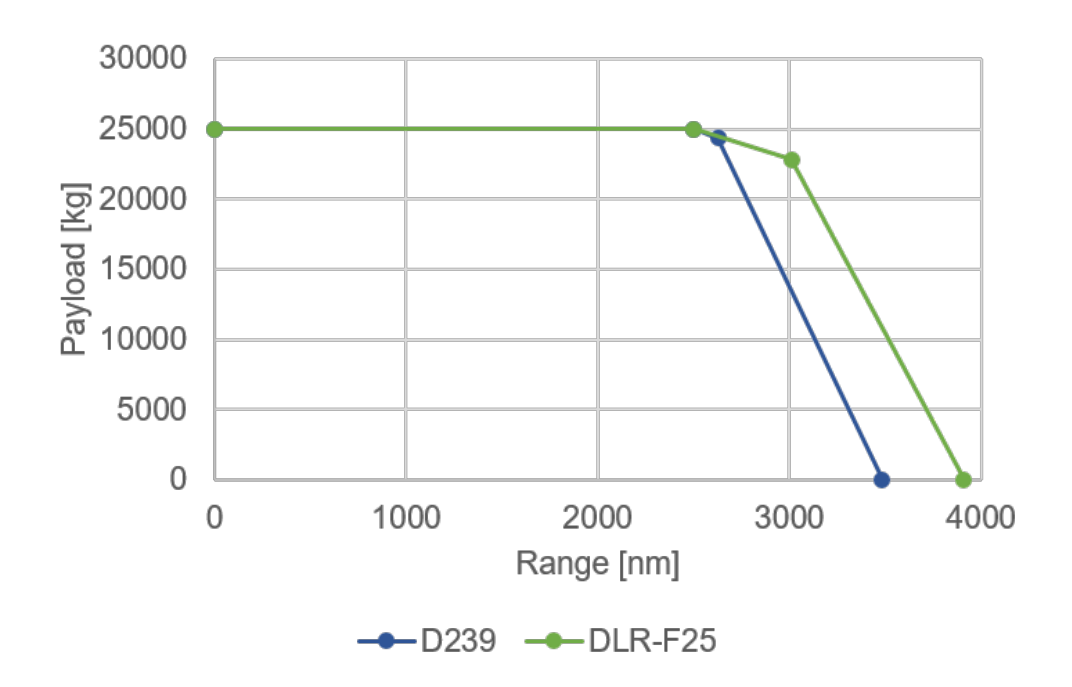


Figure 25 – Payload-range characteristic of the DLR-F25 in comparison to the D239

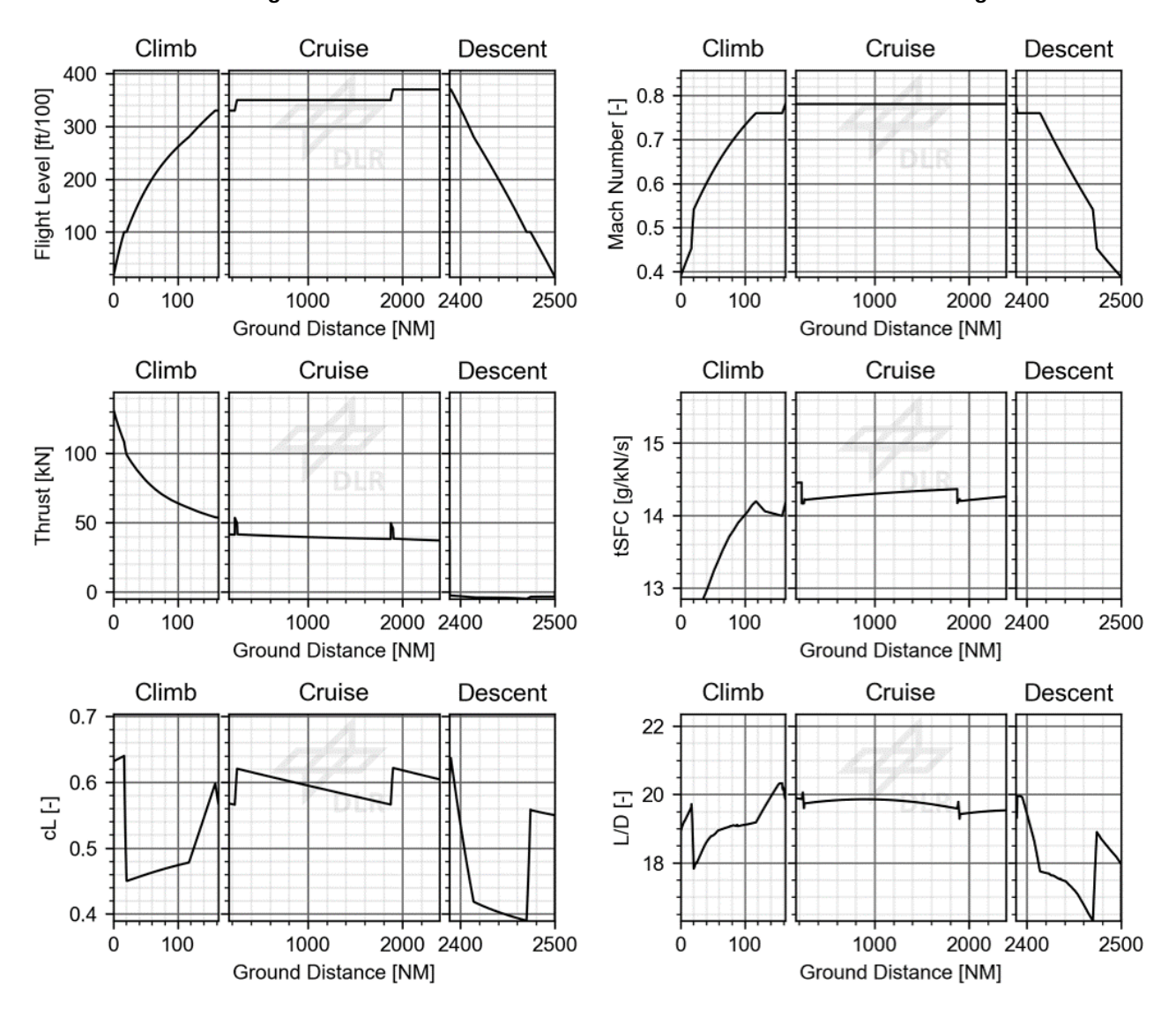


Figure 26 - Detailed flight trajectory of the design mission of the DLR-F25